

# A quantum gravitational inflationary scenario in Bianchi-I spacetime

Brajesh Gupt\* and Parampreet Singh†

*Department of Physics and Astronomy, Louisiana State University, Baton Rouge, 70803*

We investigate the  $\phi^2$  inflationary model in the Bianchi-I spacetime using the effective spacetime description of loop quantum cosmology to understand the issues of the resolution of initial singularity, isotropization, effect of anisotropies on the amount of inflation, and the phase space attractors in the presence of non-perturbative quantum gravitational modifications. A comparative analysis with the classical theory by including more general initial conditions than the ones previously considered in the latter is also performed. We show that, in general, the classical singularity is replaced by a bounce of the mean scale factor in loop quantum cosmology. Due to the underlying quantum geometric effects, the energy density of the inflaton and the anisotropic shear remain bounded throughout the non-singular evolution. Starting from arbitrary anisotropic initial conditions, a loop quantum universe isotropizes either before or soon after the onset of slow-roll inflation. We find a double attractor behavior in the phase space dynamics of loop quantum cosmology, similar to the one in classical theory, but with some additional subtle features. Quantum modifications to the dynamical equations are such that, unlike the classical theory, the amount of inflation does not monotonically depend on the initial anisotropy in loop quantum cosmology. Our results suggest that a viable non-singular inflationary model can be constructed from highly anisotropic initial conditions in the Planck regime.

## I. INTRODUCTION

The inflationary paradigm provides an excellent explanation of the homogeneity and the flatness problems of the standard model of cosmology and the origin of the observable large scale structure in our universe. However, various questions about the physics of the pre-inflationary stage of the universe remain unanswered. In particular, in general relativity (GR), inflationary spacetimes have been shown to be past incomplete [1], and little is known about the initial conditions and the geometry of the pre-inflationary epoch. Both of these issues need to be carefully addressed in any complete model of inflation. Unlike the issue of the past singularity, which can only be faithfully addressed using a quantum theory of gravity, the issue of the role of pre-inflationary geometry on the onset and predictions of inflation has been previously studied using GR (and also in modified theories of GR). In this setting, various investigations have been carried out to understand the onset of inflation in the presence of anisotropic shear in the pre-inflationary epoch, often by assuming a homogeneous and anisotropic patch of spacetime using Bianchi models [2–25]. Many results point towards isotropization and genericness of inflation starting from initial anisotropic conditions, however counter-examples have also been found (see for eg. [21, 24, 25]). Since the anisotropic shear diverges in classical gravity close to the initial singularity, it has been argued that a consistent treatment of anisotropies in the pre-inflationary epoch is incomplete without inputs from quantum gravity [9, 14]. Due to these reasons, it is important to study the pre-inflationary dynamics in a quantum gravitational anisotropic spacetime to understand the way quantum gravity effects resolve the classical singularity, and affect the isotropization and the onset of inflation in presence of anisotropies.

---

\*Electronic address: bgupt1@lsu.edu

†Electronic address: psingh@phys.lsu.edu

The goal of this article is to address these issues in loop quantum cosmology (LQC) [26], a framework to quantize homogeneous spacetimes based on loop quantum gravity (LQG). A key prediction of LQC is that the backward evolution of a universe, starting from classical initial data, by the quantum Hamiltonian constraint leads to a non-singular bounce [27–29]. The resolution of singularity in LQC is a result of the underlying discreteness of the quantum geometry at the Planck scale, and its occurrence has been confirmed in a variety of isotropic and anisotropic models (see for eg. [30–43]), including the  $\phi^2$  inflationary model in the isotropic setting [44]. A powerful tool in understanding the detailed physics of these models is the effective spacetime description of the underlying quantum dynamics [45, 46], which using sophisticated numerical simulations has been tested to the Planck curvature scale for various matter models for both isotropic [27–30, 34, 36, 38] as well as anisotropic spacetimes [47, 48] (see Refs.[49, 50] for a review of numerical methods in LQC). The effective spacetime description is derived using an effective Hamiltonian obtained via geometric methods of quantum mechanics [51], by assuming states which become semi-classical at late times, describing a macroscopic universe in the classical regime. It is found that GR is an excellent approximation to quantum dynamics at curvature scales small compared to the Planck value, however departures between the two theories become significant in the Planck regime which is described by the effective dynamics to an excellent accuracy. Using effective Hamiltonian method, bounds on expansion and shear scalars have been derived [52, 53], and generic results on the absence of strong singularities in isotropic [54, 55] and Bianchi-I spacetime [56] have been obtained.

In this manuscript, we analyze the dynamics of  $\phi^2$  inflation model in the Bianchi-I spacetime in the effective spacetime description of LQC. We first show that unlike in the classical Bianchi-I model, the past evolution in LQC is non-singular. Singularity resolution is confirmed for a large set of initial conditions, in confirmation with the generic result on resolution of singularities in Bianchi-I spacetime in LQC [56]. In contrast to the isotropic inflationary models in LQC where there is a single bounce of the isotropic scale factor [57–64] always occurring at the maximum allowed value of the energy density  $\rho_{\max} = 0.41 \rho_{\text{Pl}}$ , the resolution of singularity in Bianchi-I spacetime occurs via non-singular bounces of the three directional scale factors  $(a_1, a_2, a_3)$  occurring at a range of values of energy density and anisotropic shear scalar  $\sigma^2$ , bounded by  $\rho_{\max}$  (same as in the isotropic model) and  $\sigma_{\max}^2 = 11.57/l_{\text{Pl}}^2$ . In the isotropic LQC,  $\rho = \rho_{\max}$  at the bounce constrains the value of the inflaton velocity at the bounce for a given initial value of the inflaton field. On the other hand, in Bianchi-I spacetime in LQC, there is no such restriction. The bounce of the mean scale factor in Bianchi-I spacetime (defined as  $a = (a_1 a_2 a_3)^{1/3}$ ) can take place even if the energy density is not at its maximum value at the bounce. In this way, presence of non-vanishing shear leads to sets of initial conditions which were not allowed in the isotropic spacetime.

The availability of a non-singular inflationary model in the presence of anisotropies sets the stage to answer some important questions which so far could only be addressed within the limitations of the classical theory. These include, the way slow-roll inflation in  $\phi^2$  model begins, starting from highly anisotropic geometries; whether slow-roll inflation is an attractor of trajectories starting from arbitrary anisotropic conditions in the Planck regime; and the way non-zero anisotropic shear affects the number of e-foldings. Though these issues have been addressed to some extent earlier in the classical theory, for completeness and comparative analysis, we analyze both the classical and the effective dynamics of LQC for the  $\phi^2$  model in Bianchi-I spacetime. In the process, apart from answering the above questions in the non-singular anisotropic inflationary model in LQC, we gain new insights on some of these issues in the classical theory. Below, we summarize the main results on the study of pre-inflationary dynamics and the comparison between the classical theory and LQC.

It is known that due to the presence of anisotropic shear, the Hubble friction during cosmic expansion is enhanced which, in turn, leads to faster decay of the kinetic energy of the inflaton [20]. This helps the isotropic slow-roll conditions arrive more quickly. If the inflaton is initially taken to

roll down the potential at some initial time  $t = t_i$  ( $\dot{\phi}(t_i) < 0$ ), then due to the enhanced Hubble friction, higher anisotropy leads to an increase in the number of e-foldings. In this article, in the discussion of classical dynamics, we consider a more generic initial condition on the initial velocity of the inflaton, including the case when the inflaton is initially rolling up the potential in the pre-inflationary era. We find that, for such an initial condition i.e.  $\dot{\phi}(t_i) > 0$ , the number of e-foldings decrease with an increase in the anisotropic shear in the classical theory in comparison to the corresponding isotropic evolution. Further, in the regime of low anisotropy, there is a significant difference in the number of e-foldings depending on whether initial value of  $\dot{\phi}$  is positive or negative. In contrast, we find that the large anisotropy gives rise to the same number of e-foldings for both the signs of initial  $\dot{\phi}$ . The latter behavior of the amount of inflation can be attributed to the strength of the Hubble friction which, at large anisotropy, is so strong that the sign of  $\dot{\phi}$  becomes insignificant.

In the classical theory, for a given type of initial condition, the number of e-foldings ( $N$ ) show a monotonic variation with anisotropic shear i.e.  $N$  either decreases (for an inflaton rolling up the potential) or increases (for an inflaton rolling down the potential) with an increasing initial value of the anisotropic shear. In LQC, however, it turns out that the amount of inflation does not monotonically vary with the anisotropic shear. In the case when initial  $\dot{\phi}$  is chosen to be negative<sup>1</sup>, the number of e-foldings increase with increasing shear if the anisotropic shear scalar  $\sigma^2$  is less than a particular value  $\sigma_*^2$ , and attain a maximum value when  $\sigma^2 = \sigma_*^2$ . Thus, unlike the classical theory, there exists a range of  $\sigma^2$ :  $\sigma_*^2 < \sigma^2 \leq \sigma_{\text{max}}^2$ , for which an increase in anisotropy decreases the number of e-foldings. On the other hand, if the initial velocity of the scalar field is positive, the behavior of  $N$  is opposite. That is,  $N$  decreases for  $\sigma^2 < \sigma_*^2$ , increases if  $\sigma^2 > \sigma_*^2$  and attains a minimum value at  $\sigma^2 = \sigma_*^2$ . Interestingly, the value of  $\sigma_*^2$  turns out to be independent of whether the initial velocity of the scalar field is positive or negative (though it depends on the absolute values of initial  $\dot{\phi}$  and initial  $\phi$ ).

We also study the attractor behavior of the phase-space trajectories of the classical and LQC effective dynamics. In the classical theory, it is known that all the classical trajectories join the isotropic slow-roll inflationary trajectory in their future evolution provided the initial value of  $\phi$  is high enough to allow inflation (see for eg. [22]). Also, in the limit of initial shear scalar tending to zero, Bianchi-I trajectories approach the isotropic Friedmann-Robertson-Walker (FRW) trajectory, irrespective of the initial energy density. As in GR, it turns out that in LQC, irrespective of the initial anisotropic content of the spacetime, all the Bianchi-I spacetime trajectories, meet the isotropic slow-roll inflation in their future evolution, if the initial value of the inflaton field is high enough. In this way, slow-roll inflation is an attractor for all the trajectories in the effective spacetime of Bianchi-I LQC with a  $\phi^2$  potential starting at the bounce. Unlike in the classical theory where there exists an isotropic trajectory for every given value of energy density in the initial data, in LQC, the energy density at the bounce is fixed at  $\rho = \rho_{\text{max}}$  in the isotropic spacetime. Therefore, in order to obtain the isotropic limit of Bianchi-I spacetime in LQC at the bounce, one has to consider  $\rho \rightarrow \rho_{\text{max}}$  in addition to  $\sigma^2 \rightarrow 0$ . If the energy density at the bounce is fixed at any value other than  $\rho_{\text{max}}$  (which is allowed in Bianchi-I LQC), then it turns out, that the shear scalar can not be decreased to zero. In that case, there is a minimum non-zero value of the shear scalar, depending on the energy density at the bounce. In this sense, the approach to the isotropic limit in the effective description of LQC is subtle in comparison to the classical theory. That is, in the classical theory, isotropic spacetime can be approached by decreasing  $\sigma^2$  to zero for any fixed value of energy density in the initial data, whereas, in LQC, the energy density at the

---

<sup>1</sup> The initial conditions in most of the simulations for LQC discussed in this work are provided at the bounce of the mean scale factor.

bounce must also tend to  $\rho_{\max}$  in addition to  $\sigma^2 \rightarrow 0$ .

This manuscript is organized as follows, in section-II, we present the dynamical equations of Bianchi-I spacetime in the classical and the effective description of LQC in the Ashtekar variables. We discuss the features of anisotropic geometries, slow roll parameters, conditions for accelerated expansion, and behavior of equation of state of the scalar field in the classical theory. Based on the modified dynamical equations we discuss some key properties of the mean Hubble rate and the shear scalar in the effective description of LQC. In section-III, we discuss the numerical studies of the model where we present the results of various numerical simulations of classical and the LQC dynamics. In all the simulations, the mass of the inflaton is fixed to  $m = 1.21 \times 10^{-6} m_{\text{Pl}}$ , consistent with the WMAP data [65]. With the help of explicit numerical simulations, we show the occurrence of non-singular bounces for various values of initial anisotropic shear in the effective dynamics of Bianchi-I spacetime. We explore the process of isotropization, behavior of the number of e-foldings for various initial conditions and study the phase space trajectories of the classical and LQC Bianchi-I spacetime. To discuss the qualitative behavior of trajectories, the initial value of inflaton in various plots is taken as  $\phi = 3.14 m_{\text{Pl}}$ . Since this initial value is also required in the classical isotropic inflationary model for sufficient number of e-foldings, it serves as a good representative of the inflationary trajectories to study the effects of presence of anisotropy on the amount of inflation as compared to the classical isotropic slow-roll. Summary of results from various other initial values of the inflaton is presented in the tabular form, in Tables- I and II. We summarize with the discussion of results in Sec. V.

## II. CLASSICAL AND EFFECTIVE DYNAMICS: BASIC EQUATIONS

In this section we present the description of Bianchi-I spacetime in terms of the loop quantum variables – the Ashtekar-Barbero connection  $A_a^i$  and the triads  $E_i^a$ . In the following, the first subsection is devoted to the classical theory. After discussing the relationship of connection and triad variables with the metric variables, we outline the derivation of classical dynamical equations from the Hamiltonian constraint, and discuss in detail the conditions for accelerated expansion in the classical Bianchi-I spacetime sourced with a  $m^2 \phi^2$  inflationary potential (with  $m = 1.21 \times 10^{-6} m_{\text{Pl}}$ ). In the second subsection we outline the derivation of effective dynamical equations in the effective spacetime description of Bianchi-I spacetime in LQC, and note key non-trivial features in comparison to the classical theory which play an important role in distinctions of dynamical behavior of trajectories in GR and LQC.

### A. Classical theory

We consider a homogeneous Bianchi-I spacetime with the spatial manifold having the topology  $\Sigma (= \mathbb{R}^3)$ , thus endowing  $\Sigma \times \mathbb{R}$  topology to the spacetime manifold. The metric for Bianchi-I spacetime is given as

$$ds^2 = -N^2 dt^2 + a_1^2 dx^2 + a_2^2 dy^2 + a_3^2 dz^2, \quad (2.1)$$

where  $a_i$  denote the directional scale factors. In order to define a symplectic structure on the manifold we need to introduce a fiducial cell  $\mathcal{V}$  on the spatial manifold of the spacetime, with fiducial volume  $V_o = l_1 l_2 l_3$ . Here  $l_i$  denote the co-ordinate lengths in the three spatial directions. The edges of the fiducial cell are chosen to lie along the fiducial triads  $\hat{e}_a^i$ . The fiducial metric compatible with the fiducial co-triads  $\hat{\omega}_a^i$  is denoted as  $\hat{q}_{ab}$ .

Utilizing the underlying symmetries of the homogeneous spatial manifold of Bianchi-I spacetime, the connection  $A_a^i$  and triads  $E_i^a$  can be written in terms of the symmetry reduced connections ( $c_i$ )

and triads ( $p_i$ ) as

$$A_a^i = c^i(l_i)^{-1} \mathring{\omega}_a^i \quad \text{and} \quad E_i^a = p_i(l_i) V_o^{-1} \sqrt{\mathring{q}}, \quad (2.2)$$

where  $\mathring{q} = \det(\mathring{q}_{ab})$  is the determinant of the fiducial metric and the index  $i$  runs from 1 to 3. The symmetry reduced connection  $c_i$  and triad  $p_j$  are conjugate to each other and they satisfy the following Poisson bracket relation

$$\{c^i, p_j\} = 8\pi G \gamma \delta_j^i, \quad (2.3)$$

where  $\gamma = 0.2375$  is the Barbero-Immirzi parameter whose value is fixed using the black-hole entropy computation in LQG. The triads  $p_i$  are kinematically related to the usual metric variables of the spacetime in the following manner,

$$p_1 = \varepsilon_1 l_2 l_3 |a_2 a_3|, \quad p_2 = \varepsilon_2 l_1 l_3 |a_1 a_3|, \quad p_3 = \varepsilon_3 l_1 l_2 |a_1 a_2| \quad (2.4)$$

where  $\varepsilon_i = \pm 1$  depending on whether the triads have positive or negative orientation. In the following, without any loss of generality, we choose  $\varepsilon_i = +1$ , and the coordinate lengths  $l_i$  to be unity.

### 1. Dynamical equations

The classical Hamiltonian constraint for Bianchi-I spacetime, with lapse  $N = 1$ , in terms of the connections  $c_i$  and triads  $p_j$  can be written as follows [40]

$$\mathcal{H}_{\text{cl}} = -\frac{1}{8\pi G \gamma^2 V} (c_1 c_2 p_1 p_2 + \text{cyclic terms}) + \mathcal{H}_{\text{matt}}, \quad (2.5)$$

where  $V = \sqrt{p_1 p_2 p_3}$  stands for the physical volume of the cell  $\mathcal{V}$  and  $\mathcal{H}_{\text{matt}}$  denotes the Hamiltonian of the matter sector. Considering the form of the self interacting potential given via  $V(\phi) = \frac{1}{2} m^2 \phi^2$ , the matter Hamiltonian of the system can be written as

$$\mathcal{H}_{\text{matt}} = \frac{P_\phi^2}{2\sqrt{p_1 p_2 p_3}} + \frac{1}{2} m^2 \phi^2 \sqrt{p_1 p_2 p_3}, \quad (2.6)$$

where  $P_\phi$  is the conjugate momentum of the scalar field  $\phi$ . Starting from the total classical Hamiltonian constraint, the dynamical equations can be derived using Hamilton's equations of motion

$$\begin{aligned} \dot{p}_i &= \{p_i, \mathcal{H}_{\text{cl}}\} = -8\pi G \gamma \frac{\partial \mathcal{H}_{\text{cl}}}{\partial c_i}, \\ \dot{c}_i &= \{c_i, \mathcal{H}_{\text{cl}}\} = 8\pi G \gamma \frac{\partial \mathcal{H}_{\text{cl}}}{\partial p_i}. \end{aligned} \quad (2.7)$$

Further, the directional Hubble rates are given in terms of the time derivatives of the triads  $p_i$  as follows:

$$H_1 = \frac{1}{2} \left( \frac{\dot{p}_2}{p_2} + \frac{\dot{p}_3}{p_3} - \frac{\dot{p}_1}{p_1} \right), \quad (2.8)$$

and similarly for  $H_2$  and  $H_3$ . Using the equations of motion and the expression for the directional Hubble rates it is now straightforward to write the classical Einstein's equations for Bianchi-I spacetime as

$$\begin{aligned} H_1 H_2 + H_2 H_3 + H_3 H_1 &= 4\pi G (\dot{\phi}^2 + m^2 \phi^2), \\ \dot{H}_2 + \dot{H}_3 + H_1^2 + H_2^2 + H_3^2 &= -4\pi G (\dot{\phi}^2 - m^2 \phi^2), \end{aligned} \quad (2.9)$$

and the cyclic permutation of these two equations. Equations of motion for the scalar field can also be derived in a similar fashion which yield the Klein-Gordon equation,

$$\ddot{\phi} + 3H\dot{\phi} + V_{,\phi} = 0, \quad (2.10)$$

where  $H = (H_1 + H_2 + H_3)/3$  is the mean Hubble rate and  $V_{,\phi}$  is the derivative of the self interacting potential with respect to the field  $\phi$ . The Klein-Gordon equation governing the evolution of the scalar field is equivalent to the conservation equation  $\dot{\rho} = -3H(\rho + P)$ , where  $\rho = \dot{\phi}^2/2 + V(\phi)$  is the energy density and  $P = \dot{\phi}^2/2 - V(\phi)$  is the pressure of the scalar field. In the inflationary scenario, the term  $3H\dot{\phi}$ , also known as Hubble friction, plays an important role by causing the slow-roll of the inflaton in an expanding universe. A bigger friction term results in faster decay of the kinetic energy of the inflaton thus leading to an early start of the slow-roll conditions. This turns out to be the key to understanding the effect of the anisotropy on the amount of inflation obtained, as the anisotropic shear interacts with the dynamics of the scalar field through eq. (2.10).

The anisotropic shear is measured by a scalar  $\sigma^2$  which in terms of the directional Hubble rates is given as

$$\sigma^2 = \frac{1}{3} \left( (H_1 - H_2)^2 + (H_2 - H_3)^2 + (H_3 - H_1)^2 \right). \quad (2.11)$$

Using the expression of shear scalar  $\sigma^2$ , the vanishing of the Hamiltonian constraint  $\mathcal{H}_{\text{cl}} \approx 0$ , results in the generalized Friedmann equation for diagonal Bianchi-I spacetime:

$$H^2 = \frac{8\pi G}{3} \rho + \frac{1}{6} \sigma^2. \quad (2.12)$$

Further, using Einstein's equations for diagonal Bianchi-I spacetime (given by eq. (2.9)) one can derive the Raychaudhuri equation as follows

$$\frac{\ddot{a}}{a} = -\frac{4\pi G}{3} (\rho + 3P) - \frac{1}{3} \sigma^2. \quad (2.13)$$

Eq. (2.13) can also be obtained by computing the time derivative of the Friedmann equation given by eq. (2.12) and utilizing the conservation equation  $\dot{\rho} = -3H(\rho + P)$  along with  $\dot{\sigma}^2 = -6H\sigma^2$  [66, 67]. Note that in the classical theory,  $\sigma^2 \propto a^{-6}$ .

## 2. Kasner exponents and Jacobs' parameter

To understand the structure of spacetime in the very early stage of evolution (including the pre-inflationary epoch), it is convenient to use the Kasner exponents,  $k_i$ , which are related to the directional scale factors via  $a_i \propto t^{k_i}$ . The Kasner exponents have been extensively used to understand structure of the spatial geometry during the approach to classical singularity, which can be classified into point, barrel, pancake and cigar types. When all the Kasner exponents are positive ( $k_1, k_2, k_3 > 0$ ), then all the directional scale factors approach singularity together and the spatial geometry of the spacetime tends to a point like structure. Similarly, the approach to singularity is pancake when two of the Kasner exponents are zero and one of them is positive ( $k_1, k_2 = 0$  and  $k_3 > 0$ ), barrel, when one of the exponents is zero while other two positive ( $k_1 = 0, k_2, k_3 > 0$ ), and cigar, when one of the exponents is negative and two of them are positive ( $k_1 < 0$  and  $k_2, k_3 > 0$ ).

Using the definition of the shear scalar ( $\sigma^2$ ) and the expansion scalar  $\theta = H_1 + H_2 + H_3$ , one can write the quantity  $\sigma^2/\theta^2$  in terms of the Kasner exponents as follows

$$\frac{\sigma^2}{\theta^2} = \frac{2}{3} (1 - 3(k_1 k_2 + k_2 k_3 + k_3 k_1)). \quad (2.14)$$

The ratio of the shear scalar and the expansion scalar takes the minimum value when all of the three directions of the spacetime are expanding i.e. all the three Kasner exponents are positive. It can be easily proved that if  $\sigma^2/\theta^2 < 1/6$ , then the only solution possible is that of all of the Kasner exponents are positive. This corresponds to a point-like approach to the classical singularity in the backward evolution. Similarly, pancake type structure is characterized by  $\sigma^2/\theta^2 = 2/3$ , the cigar type structure takes place when  $\sigma^2/\theta^2 > 1/6$  and the barrel type structure is formed when  $1/6 \leq \sigma^2/\theta^2 < 2/3$ . Thus,  $\sigma^2/\theta^2$  describes a hierarchy of the spatial geometry based on the anisotropic shear present in the spacetime [68]. Since the expression for  $\sigma^2/\theta^2$  does not assume any particular form of matter, the spatial structure of the geometry given by eq. (2.14) holds true irrespective of the matter content. As an example, for the inflationary spacetime, if  $\sigma^2/\theta^2 < 1/6$  in the future evolution, then all the Kasner exponent must take positive values and hence all the directions of the spacetime must be expanding.

For the simplicity of the following calculations, we use the Jacobs' parameter  $\epsilon_J = \sigma/(4\pi G\rho)^{1/2}$  [67]. The parameter  $\epsilon_J$  denotes the dominance of the anisotropic shear over the matter density. A large value of  $\epsilon_J$  refers to a highly anisotropic universe while  $\epsilon_J \rightarrow 0$  corresponds to isotropization (i.e. when the contribution of matter density to the spacetime curvature is far greater than that of the anisotropic shear). Moreover, the value of  $\epsilon_J$  can be related to the structure of the spatial geometry near the classical singularity. As an example, for  $\epsilon_J < 2/\sqrt{3}$  (which corresponds to  $\sigma^2/\theta^2 < 1/6$ ), all the directional Hubble rates are necessarily positive and the approach to singularity in the backward evolution is point like. For very large anisotropy, with  $\epsilon_J \gg 2/\sqrt{3}$ , the approach to singularity is cigar like. For a detailed discussion on the relation between anisotropy and the hierarchy of the approach to classical singularity in diagonal Bianchi-I spacetime, see Ref. [68].

### 3. Accelerated expansion

The condition for an accelerated expansion in terms of the equation of state and the parameter  $\epsilon_J$  can be obtained by putting the condition  $\ddot{a}/a > 0$  in the Raychaudhuri equation (eq. (2.13)) for Bianchi-I spacetime. It yields:

$$w < -\frac{1 + \epsilon_J^2}{3}, \quad (2.15)$$

where  $w = P/\rho$  is the varying equation of state of the scalar field. For  $\epsilon_J = 0$  the above expression reduces to the condition for inflation in isotropic spacetime ( $w < -1/3$ ).

According to the inequality (2.15), whether or not a Bianchi-I universe undergoes accelerated expansion depends on the position of the field in the inflationary potential and also on the anisotropic shear in the universe. This is in contrast to the isotropic model, where the position of the inflaton in the inflationary potential is sufficient to determine whether the expansion of the universe accelerates or not. We demonstrate this in Fig. 1, which shows two plots depicting the validity of the inequality given in eq. (2.15). In this figure, the initial values specified at  $t = 0$  are :  $\dot{\phi}(0) = -2 \times 10^{-5} m_{\text{Pl}}^2$  and  $\phi(0) = 3.14 m_{\text{Pl}}$ . (The qualitative behavior of the plot remains the same for other values of initial  $\dot{\phi}$  and  $\phi$ ). We choose  $\phi(0) = 3.14 m_{\text{Pl}}$ , just as a representative value to discuss the behavior of inflationary trajectories, as this value is close to the value of the inflaton field near the onset of slow-roll in the isotropic spacetime, to generate approximately 60 e-foldings. In the rest of the article, unless a different initial condition is specified, we will take  $\phi(0) = 3.14 m_{\text{Pl}}$ , wherever required to discuss qualitative behavior of amount of inflation and dynamical trajectories, shown in the plots in the following sections. The left plot in Fig. 1 is for a small value of initial anisotropic shear and the right one corresponds to a higher anisotropic shear. In these plots, the

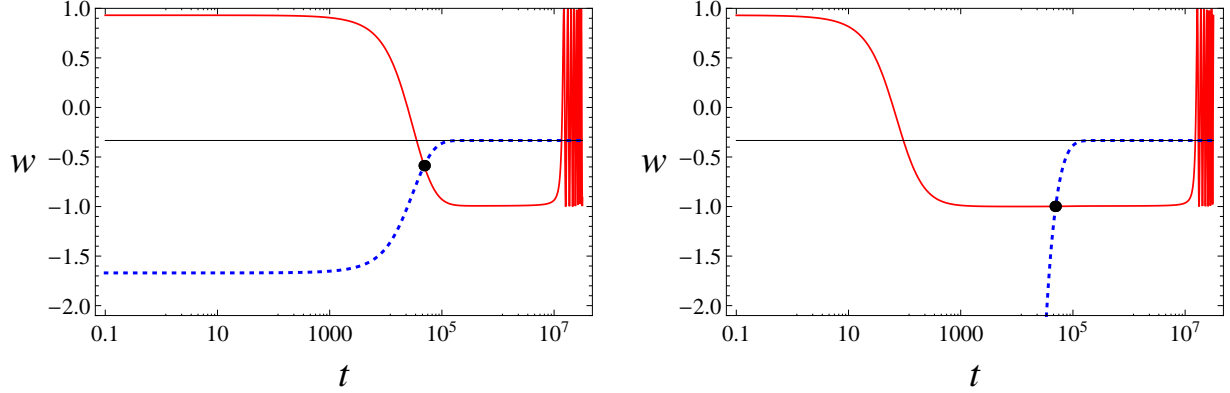


FIG. 1: In this figure the (red) solid curve shows the equation of state, the (blue) dashed curve denotes  $-(1 + \epsilon_J^2)/3$ , the thin black horizontal line shows the  $w = -1/3$  line and the black dot marks the onset of accelerated expansion (inflation). The accelerated expansion starts when equation of state satisfies the condition given by eq. (2.15). The initial data for these plots are  $\dot{\phi}(0) = -2 \times 10^{-5} m_{\text{Pl}}^2$  and  $\phi(0) = 3.14 m_{\text{Pl}}$ , with  $\epsilon_J^2(0) = 4.01$  for the left, and  $\epsilon_J^2(0) = 1.17 \times 10^5$  for the right plot. The mass of the inflation is taken to be  $m = 1.21 \times 10^{-6} m_{\text{Pl}}$ .

initial conditions are taken such that the kinetic energy is greater than potential energy and the equation of state is initially<sup>2</sup>  $w \approx 1$ . As the further evolution takes place, the kinetic energy decays and the equation of state decreases. After some time, the potential energy dominates over the kinetic energy and the equation of state becomes  $w \approx -1$ . In the right plot of Fig. 1, we see that though the equation of state  $w$  attains the value  $-1$  quite early, around  $t \approx 1,000 t_{\text{Pl}}$ , but, the accelerated expansion does not start until eq. (2.15) is satisfied, which occurs around  $t \approx 50,000 t_{\text{Pl}}$ . In contrast, in the left plot since the initial anisotropic shear is weak, the accelerated expansion starts close to  $w < -1/3$ .

Using eq. (2.15), one may be tempted to conclude that a non-vanishing value of the parameter  $\epsilon_J$  is detrimental to the amount of inflation in comparison to the isotropic model, since more negative value of the equation of state is required for an accelerated expansion of the universe. However, as earlier pointed out in Ref. [20], this expectation turns out to be incorrect. It turns out that the presence of anisotropy actually helps inflation by increasing the Hubble rate, which in turn enhances the friction term ( $3H\dot{\phi}$ ) in the Klein-Gordon equation. Due to this enhanced Hubble friction, the kinetic energy of the scalar field decays at a faster rate. This brings the condition for accelerated expansion to be achieved earlier, in presence of anisotropy, causing a longer phase of accelerated expansion.

The condition for accelerated expansion can also be written in terms of the contributions from kinetic and potential energies, and the shear scalar, by using eq. (2.13). Substituting the expressions for energy density and pressure in terms of the kinetic ( $\dot{\phi}^2/2$ ) and potential energy  $V(\phi)$ , eq. (2.13) yields,

$$\frac{\ddot{a}}{a} = -\frac{4\pi G}{3} \left( 2\dot{\phi}^2 - 2V(\phi) + \frac{\sigma^2}{4\pi G} \right). \quad (2.16)$$

<sup>2</sup>By starting with kinetic dominated initial conditions we make sure that we start with conditions not favorable for inflation to occur immediately. The initial trajectory, although away from the inflationary trajectory, joins the inflationary trajectory in the forward evolution (as discussed later in this article).



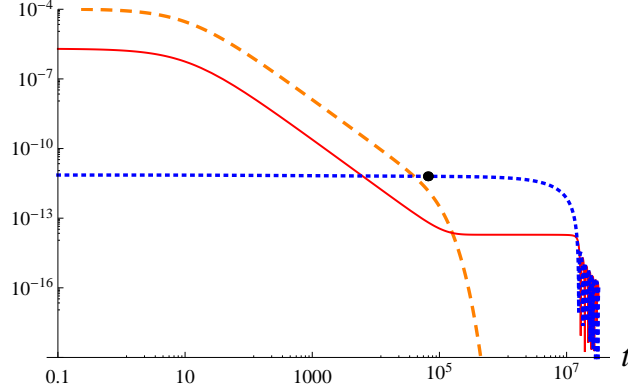


FIG. 2: This figure shows the evolution of kinetic ( $\dot{\phi}^2/2$ ), potential ( $m^2\phi^2/2$ ) and anisotropic shear ( $\sigma^2/16\pi G$ ) terms with time. The (red) solid curve shows the kinetic energy contribution, the (blue) short dashed curve corresponds to potential energy contribution, and the (orange) dashed curve shows the shear term. The black dot marks the onset of inflation. Inflation takes place in the regime when potential energy dominates over the kinetic energy as well as the shear term.

The condition for accelerated expansion can then be written as:

$$V(\phi) > 2 \left( \frac{\dot{\phi}^2}{2} + \frac{\sigma^2}{16\pi G} \right).$$

This relation tells us that for inflation (accelerated expansion) to take place, the potential energy must dominate both the kinetic energy and the anisotropic shear term in the above equation. In Fig. 2, we show the evolution of the kinetic and potential energy, and  $\sigma^2/16\pi G$  with respect to time. It is evident that inflation does not start (denoted by a black dot in Fig. 2), until the sum of shear term  $\sigma^2/16\pi G$  and the kinetic energy term becomes less than half of the potential term. We also see that following the onset of inflation, there is a short period where the shear term dominates over the kinetic energy, before it decays quickly during accelerated expansion. Thus, there may be a short duration of anisotropy during the classical inflationary phase of Bianchi-I spacetime. However, this is not a generic feature of evolution in Bianchi-I spacetime. If the initial conditions are such that the shear energy is less than the kinetic energy in the beginning, then there will not be any duration of such dominance of shear over kinetic energy.

For the subsequent discussion of the numerical results, it is useful to define the slow-roll parameters. In the classical isotropic inflationary spacetime, the slow-roll parameters  $\epsilon$  and  $\eta$  are defined as

$$\epsilon = 3 \frac{\dot{\phi}^2}{\dot{\phi}^2 + 2V(\phi)} \quad \text{and} \quad \eta = -\frac{\ddot{\phi}}{H\dot{\phi}}. \quad (2.17)$$

The slow-roll inflation is defined as the phase of evolution where  $\epsilon, |\eta| \ll 1$ . Smallness of these parameters implies that the Hubble rate ( $H$ ) varies very slowly. In the discussion of the numerical results, we consider above definition of slow-roll parameters in the inflationary Bianchi-I spacetimes.

It is evident from the eq. (2.17) that for small slow-roll parameters,  $\epsilon, |\eta| \ll 1$ , the value of both  $\dot{\phi}$  and  $\ddot{\phi}$  will be small. This implies that during the slow-roll phase, the inflaton rolls down the potential with a small and almost constant velocity. An example of the numerical evolution of  $\epsilon$  and  $\dot{\phi}$ , in Bianchi-I spacetime, starting from  $\phi(0) = 3.14 m_{\text{Pl}}$ ,  $\dot{\phi}(0) = 0.00002 m_{\text{Pl}}^2$  and  $\epsilon_J^2(0) = 1.58 \times 10^{14}$ , is shown in Fig. 3. We see that, once  $\epsilon \ll 1$ , the slow-roll inflation sets in, and the field

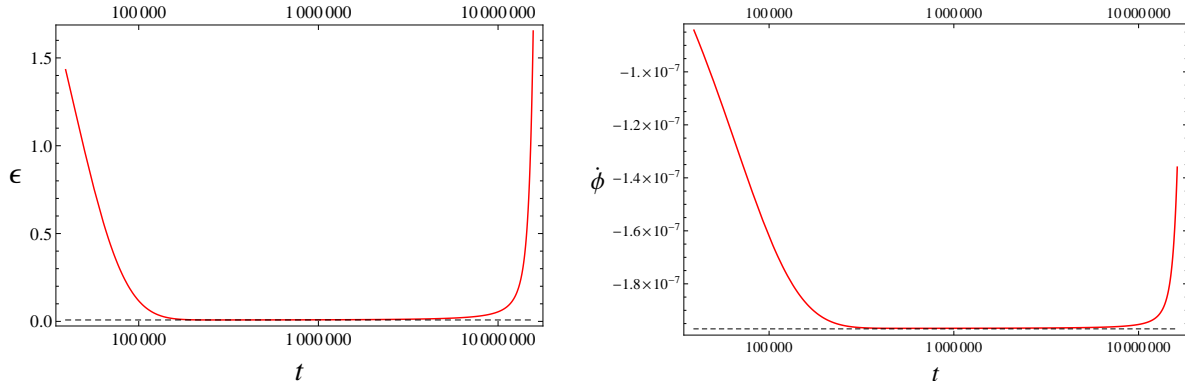


FIG. 3: This figure shows an example of the evolution of the slow-roll parameter  $\epsilon$  and corresponding field velocity  $\dot{\phi}$ . The dashed black line in the left plot marks  $\epsilon \approx 0.008$  and in the right plot it shows the corresponding value of the field velocity  $\dot{\phi} \approx 1.97 \times 10^{-7} m_{\text{Pl}}^2$ . The initial conditions are taken as  $\phi(0) = 3.14 m_{\text{Pl}}$ ,  $\dot{\phi}(0) = 0.00002 m_{\text{Pl}}^2$  and  $\epsilon_J^2(0) = 1.58 \times 10^{14}$ . It is clearly seen that even for initial anisotropy as high as  $\epsilon_J^2(0) = 1.58 \times 10^{14}$ , the slow-roll conditions are met in the future evolution.

velocity varies very slowly. For these initial conditions, during this phase, the value of velocity of the inflaton is  $\dot{\phi} \approx 1.97 \times 10^{-7} m_{\text{Pl}}^2$  and the slow-roll parameter is  $\epsilon \approx 0.008$ .

## B. LQC Effective equations

Canonical quantization of cosmological models in LQC is based on techniques in LQG. The classical gravitational Hamiltonian constraint of a given model is first expressed in terms of the holonomies of connections  $A_i^a$  and fluxes of the triads  $E_a^i$ , which are then expressed as appropriate quantum operators. The quantum Hamiltonian constraint hence obtained gives rise to a non-singular quantum difference equation [26]. Based on the geometric formulation of quantum mechanics, an approximate continuous description of the underlying quantum geometry, known as the effective description of LQC, can be obtained through a faithful embedding of the classical phase space into the quantum phase space of LQC [51]. Through an appropriate choice of semiclassical states, those which correspond to a macroscopic universe at late times, an effective Hamiltonian constraint can be derived by calculating the leading order corrections introduced by the underlying discrete geometry of the spacetime [45, 46]. The effective Hamiltonian constraint hence obtained gives rise to the modified equations of motion, which introduce corrections to the classical Friedmann and Raychaudhuri equations. Extensive numerical simulations for various matter models, including the Bianchi-I anisotropic spacetimes, by considering the LQC evolution of a semi-classical states show that the effective theory agrees very well with the full quantum dynamics at almost all scales, including the deep Planck regime and the classical low curvature regime [28–30, 33, 34, 36, 38, 47–50].

The effective Hamiltonian constraint for the Bianchi-I spacetime, with lapse  $N = 1$ , is given via [39, 69–71]<sup>3</sup>

<sup>3</sup> The effective Hamiltonian considered here does not incorporate “inverse triad corrections” which are only meaningful in the models with a compact topology. As mentioned earlier, the topology for the Bianchi-I spacetime, assumed to be  $\Sigma \times \mathcal{R}$ , is non-compact in the present context. Even if one considers a compact topology, since the physical volume of the fiducial cells in the numerical simulations remain large compared to the Planck volume, the corrections due to the inverse triad terms would be negligible.

$$\mathcal{H}_{\text{eff}} = -\frac{1}{8\pi\gamma^2 V} \left( \frac{\sin(\bar{\mu}_1 c_1)}{\bar{\mu}_1} \frac{\sin(\bar{\mu}_2 c_2)}{\bar{\mu}_2} p_1 p_2 + \text{cyclic terms} \right) + \mathcal{H}_{\text{matt}}, \quad (2.18)$$

where  $V = \sqrt{p_1 p_2 p_3}$  is the physical volume,  $\mathcal{H}_{\text{matt}}$  is the matter Hamiltonian taken to be same as given in eq. (2.6) and  $\bar{\mu}_i$  are lengths of the plaquette around which the holonomies are calculated [39].<sup>4</sup>

$$\bar{\mu}_1 = \lambda \sqrt{\frac{p_2 p_3}{p_1}}, \quad \bar{\mu}_2 = \lambda \sqrt{\frac{p_1 p_3}{p_2}} \quad \text{and} \quad \bar{\mu}_3 = \lambda \sqrt{\frac{p_2 p_1}{p_3}}. \quad (2.19)$$

Here  $\lambda^2 = 4\sqrt{3}\pi\gamma l_{\text{Pl}}^2$  denotes the minimum area gap which results from the quantum discreteness of spatial geometry in LQG.

The effective Hamiltonian constraint given via eq. (2.18) generates the dynamics of the spacetime for a given matter part of the Hamiltonian constraint,  $\mathcal{H}_{\text{matt}}$ . The equations of motion of the triads and the connections are given via the Hamilton's equation of motion for  $\mathcal{H}_{\text{eff}}$  (see for eg. [56]):

$$\dot{p}_1 = \frac{p_1}{\gamma\lambda} (\sin(\bar{\mu}_3 c_3) + \sin(\bar{\mu}_2 c_2)) \cos(\bar{\mu}_1 c_1) \quad (2.20)$$

and

$$\begin{aligned} \dot{c}_1 = & \frac{1}{\gamma\lambda p_1} \left[ \cos(\bar{\mu}_2 c_2) (\sin(\bar{\mu}_1 c_1) + \sin(\bar{\mu}_3 c_3)) c_2 p_2 + \cos(\bar{\mu}_3 c_3) (\sin(\bar{\mu}_1 c_1) + \sin(\bar{\mu}_2 c_2)) c_3 p_3 \right. \\ & \left. - \cos(\bar{\mu}_1 c_1) (\sin(\bar{\mu}_2 c_2) + \sin(\bar{\mu}_3 c_3)) c_1 p_1 - \frac{2\bar{\mu}_1 p_2 p_3}{\lambda} \right. \\ & \left. (\sin(\bar{\mu}_2 c_2) \sin(\bar{\mu}_3 c_3) + \text{cyclic terms}) \right] + 8\pi G\gamma \frac{\partial \mathcal{H}_{\text{matt}}}{\partial p_1}. \end{aligned} \quad (2.21)$$

The equations of motion of other directional triads and connections can also be computed in a similar fashion. The equations of motion hence obtained, along with the initial data which satisfies the effective Hamiltonian constraint given by eq. (2.18), lead to a well posed initial value problem. The dynamical equations obtained from the effective Hamiltonian constraint modify the classical Einstein's field equations in a significant way. It is evident from eq. (2.20) that  $\dot{p}_i/p_i$  never diverges during the evolution as the value of  $\sin(\bar{\mu}_i c_i)$  and  $\cos(\bar{\mu}_i c_i)$  are bounded above by unity. This further leads to non-diverging curvature scalars of Bianchi-I spacetimes such as energy density ( $\rho$ ), shear ( $\sigma^2$ ) and expansion ( $\theta$ ) scalars for the comoving observers which are bounded above by their respective maxima [53]. These values are given by:

$$\rho_{\text{max}} \approx 0.41\rho_{\text{Pl}}, \quad \theta_{\text{max}} \approx \frac{2.78}{l_{\text{Pl}}}, \quad \text{and} \quad \sigma_{\text{max}}^2 \approx \frac{11.57}{l_{\text{Pl}}^2}.$$

Moreover, it has been shown that all the curvature invariants of Bianchi-I spacetime are bounded and all the strong singularities of Bianchi-I spacetime, for the matter satisfying null energy condition, are resolved [56]. The resolution of singularity results in a non-singular bounce in the evolution of Bianchi-I spacetime in the effective description of LQC. Far way from Planckian regime, where the spacetime curvature is small, the effective dynamical trajectory agrees well with the classical theory. In the backward evolution as the spacetime curvature grows, the effective trajectory differs from the classical trajectory. During the subsequent backward evolution the classical trajectory

---

<sup>4</sup> Sometimes in literature, one finds a different functional dependence of  $\bar{\mu}_i$  on triads. It turns out that the form  $\mu_i(p_1, p_2, p_3)$  given by the equation above is the only known choice where resulting physics is independent of the rescaling freedoms of the fiducial cell when the manifold is non-compact (see ref. [52] for details).

goes into singularity, whereas the effective dynamical trajectory undergoes a non-singular bounce. In the effective dynamical evolution, the curvature scalars are always finite and bounded by their respective maxima given in the above equation.

The finite and non-diverging values of the curvature scalars introduce interesting modifications in terms of the choice of initial conditions and the dynamics of the evolution of universe in the pre-inflationary regime in the Bianchi-I spacetime in LQC. There are two important modifications relevant to our discussion.

- Unlike in the classical theory, it turns out that in LQC, the mean Hubble rate does not monotonically vary with the shear scalar. This behavior has been noted for the first time in the numerical simulations discussed in this paper<sup>5</sup>. Due to such a non-monotonic behavior of the Hubble rate as a function of the shear scalar, the Hubble friction in the Klein-Gordon equation is affected in a similar fashion. In other words, unlike in the classical theory, *Hubble friction is not always enhanced by the anisotropic shear in LQC*.
- The shear scalar in LQC during the pre-inflationary regime behaves very differently than that in the classical theory. Unlike in the classical theory, where  $\sigma^2 \propto a^{-6}$ , shear scalar does not have a monotonic dependence on the scale factor, near the bounce. There may be instances when, depending on the conditions at the bounce, the shear scalar starts out with a very small value, and then increases to reach a local maxima. On the subsequent evolution, the shear scalar would decrease and approach the classical value in the regime where quantum gravity corrections are weak. As we will see in next section, this has important implications in regards to the isotropic limit and the attractor behavior of Bianchi-I spacetime in the vicinity of the bounce.

### III. CLASSICAL AND EFFECTIVE DYNAMICS: NUMERICAL RESULTS

In this section we present numerical studies of the Bianchi-I spacetime with an inflaton as a matter field with a self-interacting potential  $V(\phi) = m^2\phi^2/2$ . In the first subsection, we discuss the results of the classical theory and the following subsection is devoted to the numerical simulations of the effective spacetime description in LQC. We discuss important features of both the classical and the LQC descriptions of the Bianchi-I inflationary spacetime, such as the effect of anisotropic shear on the amount of inflation, the process of isotropization, the isotropic limit of Bianchi-I spacetime, and the attractor behavior. Over a hundred simulations were performed for both the classical theory and LQC by varying different parameters including the initial shear scalar, the initial value of the inflaton and the initial velocity of the inflaton. In all of the simulations, the mass of the inflaton is taken as  $m = 1.21 \times 10^{-6} m_{\text{Pl}}$  and the numerical accuracy of the vanishing of the Hamiltonian constraint is of the order of  $10^{-10}$ . Note that there is a symmetry associated to the signs of the value of inflaton field and its time derivative. That is, the results remain invariant if the sign of both  $\phi$  and  $\dot{\phi}$  are changed simultaneously. In the numerical simulations performed in this article, we take the initial value of the inflaton field to be positive. For an inflaton which is initially rolling down, we take  $\dot{\phi}(0) < 0$  and for an inflaton which is initially rolling up, we take  $\dot{\phi}(0) > 0$ .

---

<sup>5</sup> Due to unavailability of the modified generalized Friedmann equation for the Bianchi-I spacetime in LQC, it is difficult to obtain this result analytically. However, in the regime where anisotropic shear is weak, the modified Friedmann equation for Bianchi-I spacetime in LQC has been obtained and it contains  $\sigma^4$  corrections [69]. These corrections can cause the Hubble rate to decrease if the anisotropic shear increases beyond a certain value.

## A. Classical theory

As discussed in the previous section, the dynamics of the classical Bianchi-I spacetime is governed by the generalized Friedmann and Raychaudhuri equations (eq. (2.12) and eq. (2.13)) from where it follows that specifying the energy density, pressure and the shear scalar at a given time provides a complete initial data. For a scalar field the pressure and energy density can be expressed in terms of the value of the scalar field  $\phi$  and its time derivative  $\dot{\phi}$ . Thus, giving the initial value of the scalar field, its velocity and the shear scalar forms a complete set of information required to compute the state of the universe at any later time. We evolve the initial data provided in a pre-inflationary phase and study various properties of the dynamical trajectories including isotropization, amount of inflation and the phase-space portraits. As discussed in the previous section, inflation takes place when the potential energy dominates over the sum of kinetic energy term ( $\dot{\phi}^2/2$ ) and the shear contribution ( $\sigma^2/16\pi G$ ). In the numerical simulations presented in this section we will, however, start with a kinetic and shear dominating initial conditions. This gives insights on the way conditions in favor of inflation are achieved, starting from comparatively unfavorable initial conditions. Moreover, it brings out important features about the behavior of the pre-inflationary dynamics and its dependence on various parameters.

### 1. Isotropization: behavior of the directional scale factors

We first discuss the process of isotropization of Bianchi-I spacetime, that is the way a Bianchi-I universe starting with highly anisotropic initial conditions at the bounce with at least one scale factor contracting turns into one with all-expanding-directions. A Bianchi-I universe can evolve from highly anisotropic initial conditions which, depending on the strength of anisotropy, entail to various possible geometrical structures of the spatial geometry such as a cigar, pancake etc, close to the classical singularity. The key question is the way an inflationary spacetime with all expanding directions emerges from such a state.

Recall that the structure of the spatial geometry of the spacetime can be determined via the value of the Jacobs' parameter  $\epsilon_J$ . For example,  $\epsilon_J < 2/\sqrt{3}$  is a sufficient condition for all the directions to expand, whereas, for  $\epsilon_J \geq 2/\sqrt{3}$ , not all of the directions will be in expanding state (as shown in the left plot of Fig. 4 where one of the directions is contracting while the other two expand in the forward evolution). Thus, at the onset of inflation, depending on the value of  $\epsilon_J$ , all the directions may either be expanding or not. From the equations of motion of Bianchi-I spacetime, it is straightforward to see that the anisotropic shear ( $\sigma^2$ ) in an expanding classical Bianchi-I spacetime always decreases, as  $\sigma^2 \propto a^{-6}$ . During inflation, the mean scale factor grows exponentially which leads to a rapid decrease in  $\sigma^2$ , and hence in the value of  $\epsilon_J$ . Due to this reason,  $\epsilon_J$  quickly becomes less than  $2/\sqrt{3}$  even if it starts from a larger value. Thus, even if one starts with a large  $\epsilon_J$  in the Bianchi-I spacetime,  $\epsilon_J$  becomes less than  $2/\sqrt{3}$  either before, or shortly after, the start of inflation, and all the directional scale factors turn out to be in the expanding state.

Fig. 4 shows the evolution of the three directional scale factors starting from a cigar like structure, such that two of the scale factors are increasing while the remaining one decreases, as the universe expands. It is evident from the left plot of Fig. 4 that in the forward evolution, the decreasing scale factor undergoes a turn around shortly after the time of onset of inflation,  $t = T_{\text{ON}}$  (defined as the time where  $\ddot{a}/a$  becomes positive). After the turn around, all the scale factors undergo expansion. The adjoining right plot shows the evolution of individual Kasner exponents. In the beginning, one of the Kasner exponents, corresponding to the contracting directional scale factor, is negative which becomes positive soon after the onset of inflation.

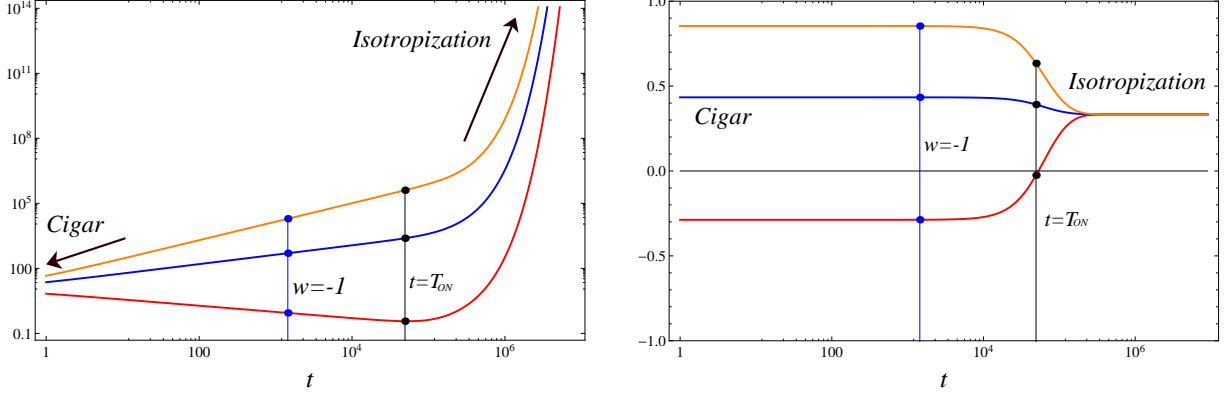


FIG. 4: The left plot shows the evolution of directional scale factors in classical Bianchi-I spacetime in the inflationary scenario. The initial data is such that backward evolution gives a cigar like singularity. It is evident that, in the forward evolution, the contracting direction undergoes a turn around near the onset of inflation and during most of the inflation all the scale factors expand. The adjoining plot shows the evolution of the corresponding Kasner exponents. Note that although  $w = -1$  is attained earlier, inflation does not begin until  $t = T_{\text{ON}}$  due to the presence of anisotropy. ( $T_{\text{ON}}$  corresponds to the time at the onset of inflation).

In a similar way, one can study the isotropization of the Bianchi-I spacetime from the barrel and pancake like structures. In these cases too, irrespective of the their initial behavior, all the directional scale factors enter expansion phase either before or soon after the onset of inflation. In this way, an inflationary Bianchi-I spacetime isotropizes, no matter what the pre-inflationary conditions are. Such a turn around of the scale factor is a feature of a generic initial data, except for those with point like structures for which all the three directions are already expanding. Similar turn around of directional scale factors and the evolution of Kasner exponents was also noted in Ref. [22].

## 2. Number of e-foldings and initial conditions

The number of e-foldings measure the amount of inflation during the inflationary era of the universe. This number is defined as  $N = \ln(a_f/a_i)$ , where  $a_f$  corresponds to the value of the mean scale factor where accelerated expansion ends, and  $a_i$  denotes the value of the mean scale factor where the accelerated expansion begins. We performed many simulations to compute the number of e-foldings for various initial values of the anisotropic shear. Fig. 5 shows the variation of the number of e-foldings as a function of the initial anisotropy (measured by  $\epsilon_J$ ), for a scalar field having a negative initial velocity ( $\dot{\phi}(0) < 0$ , corresponding to a rolling down inflaton). To discuss the qualitative behavior of the amount of inflation, in the plots shown in this article, we choose the initial value of the inflaton to be  $\phi(0) = 3.14 m_{\text{Pl}}$ . As mentioned earlier, this is just a choice representing inflationary trajectories and the way anisotropic shear affects the sufficient number of e-foldings, as this value is close to the value of inflaton at the onset of isotropic slow-roll to generate approximately 60 e-foldings in the isotropic spacetime<sup>6</sup>. The qualitative behavior discussed in this section also holds true for other values of  $\phi(0)$  for which inflation takes place. We will consider other values of  $\phi(0)$  while discussing the quantitative details of the amount of

<sup>6</sup> In order to obtain approximately 60 e-foldings in the classical isotropic spacetime, the slow-roll has to start at  $\phi \approx 3.14 m_{\text{Pl}}$  with the required value of the velocity of the inflaton being  $\dot{\phi} \approx 1.97 \times 10^{-7} m_{\text{Pl}}^2$

e-foldings. In confirmation with the known results in classical theory in this scenario, we find that if the inflaton is initially rolling down then the number of e-foldings increases with an increase in anisotropy. Further, different initial  $\dot{\phi}$ 's produce the similar number of e-foldings for large initial anisotropy. That is, the spacetime tends to achieve the same number of e-foldings for large value of initial anisotropic shear irrespective of the initial kinetic energy of the scalar field. Note that for the higher values of initial anisotropy, an inflaton which rolls down the potential without initially satisfying slow roll conditions, quickly enters into slow roll. The universe starts inflating almost exponentially, which shortens the stage of anisotropic evolution. Numerical simulations show that for high values of initial anisotropic shear, the phase of anisotropic inflation is so short that any change in anisotropy produces little effect on the number of e-foldings.

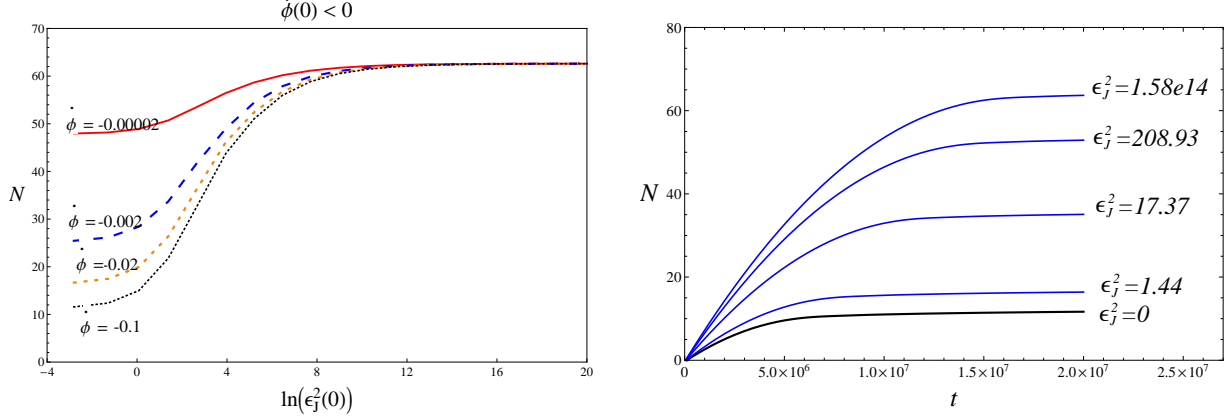


FIG. 5: The left plot in this figure shows the number of e-foldings,  $N$  plotted against the initial value of  $\ln(\epsilon_J^2)$  for various values of the initial  $\dot{\phi}$ . For each initial value of  $\dot{\phi}$ , the energy density is kept fixed while the anisotropic shear is varied. From top to bottom, curves correspond to  $\dot{\phi}(0) = (-2 \times 10^{-5}, -2 \times 10^{-3}, -2 \times 10^{-2}, -0.1) m_{\text{Pl}}^2$ . For large values of initial  $\epsilon_J$ , all the trajectories tend to produce the same number of e-foldings. The right plot shows the variation of the number of e-foldings with time for various initial anisotropy parameters  $\epsilon_J$ , but starting with the same initial value of  $\dot{\phi}$ :  $\dot{\phi}(0) = -0.1 m_{\text{Pl}}$ . In both the plots, the initial value of the inflaton field is taken as  $\phi(0) = 3.14 m_{\text{Pl}}$ .

The right plot in Fig.5 shows the evolution of the number of e-foldings during the forward evolution of inflationary Bianchi-I spacetime starting with the same  $\dot{\phi}(0) = -0.1 m_{\text{Pl}}^2$  but for the various values of the initial anisotropy parameters  $\epsilon_J$ . For these initial conditions, the number of e-foldings in the isotropic case (the case  $\epsilon_J = 0$ ) is less than 10. Whereas, in the Bianchi-I spacetime, the same initial conditions on the scalar field produce significantly more number of e-foldings for higher  $\epsilon_J$ . Thus for  $\dot{\phi}(0) < 0$ , anisotropic shear not only increases the number of e-foldings, but a large anisotropy also makes slow-roll conditions be achieved irrespective of the initial velocity of the inflaton due to an increase in the Hubble friction in the Klein-Gordon equation.<sup>7</sup>

We now consider the case of inflaton initially rolling up the potential, i.e.  $\dot{\phi}(0) > 0$ . To our knowledge, this case has not been discussed elsewhere in the literature. The left plot in the Fig.6 shows the variation of number of e-foldings with the increasing anisotropy in the initial data for various values of  $\dot{\phi}(0) = (2 \times 10^{-5}, 2 \times 10^{-3}, 2 \times 10^{-2}, 0.1) m_{\text{Pl}}^2$ . In all these simulations, the value of the inflaton field in the initial data has been taken as  $\phi(0) = 3.14 m_{\text{Pl}}$ , on the same footing as in Fig.5. In contrast to the case of inflaton rolling down the potential, it turns out that, in this case, the number of e-foldings decrease as the anisotropy in the initial data increases. For large

<sup>7</sup> In GR, irrespective of the initial inflaton velocity, one can always find a suitable value of initial anisotropic shear such that slow-roll is obtained.

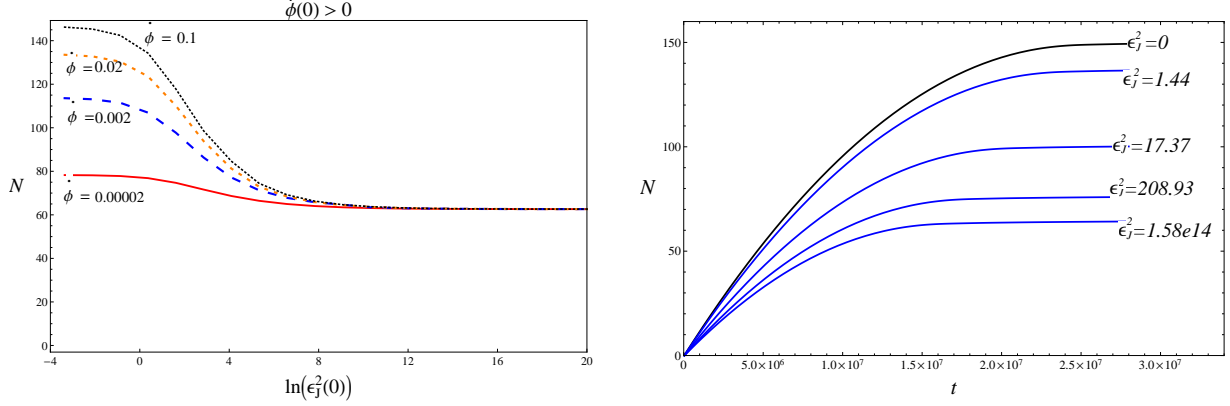


FIG. 6: This figure shows the number of e-foldings,  $N$  plotted against  $\ln(\epsilon_j^2)$  for various values of the initial  $\dot{\phi}$ . In the left plot, from bottom to top, the curves correspond to  $\dot{\phi}(0) = (2 \times 10^{-5}, 2 \times 10^{-3}, 2 \times 10^{-2}, 0.1) m_{\text{Pl}}^2$  and initial value of field is taken  $\phi(0) = 3.14 m_{\text{Pl}}$  for all the simulations. The right plot shows the time evolution of the number of e-foldings for various initial anisotropy starting with the same initial value of the inflaton velocity  $\dot{\phi}(0) = 0.1 m_{\text{Pl}}$ .

initial anisotropic shear, all the trajectories attain the same number of e-foldings irrespective of the initial  $\dot{\phi}$ .

To understand the decrease in number of e-foldings with an increase in anisotropy, let us for a moment consider the isotropic model. In the isotropic case, an initial  $\dot{\phi}(0) > 0$  causes the field to roll up the potential before the onset of inflation. For example, if the initial  $\dot{\phi}$  is say  $\dot{\phi}(0) = 0.1 m_{\text{Pl}}^2$  (with initial  $\phi$  as  $3.14 m_{\text{Pl}}$ ), then the inflaton will roll up the potential and inflation starts to take place at  $\phi \approx 4.8 m_{\text{Pl}}$ . As a result, the amount of inflation is greater as compared to the case of initial  $\dot{\phi} < 0$ . On the other hand, in Bianchi-I spacetime due to the increase in Hubble friction, there is a faster decay of the kinetic energy of the field, and the field stops its upward journey on the potential before reaching  $\phi \approx 4.8 m_{\text{Pl}}$ . Thus, inflation starts taking place at a comparatively smaller value of the field. Hence, for an inflaton which is initially rolling up the potential, an increase in anisotropy reduces the number of e-foldings in comparison to the corresponding isotropic evolution. At very large anisotropy, the Hubble friction is so strong that the kinetic energy of the field decays quickly, and inflation onsets very close to the initial value of the inflaton.

It is important to note that for a large initial anisotropy, both the positive and negative initial velocity of the field give the same amount of inflation. This is evident from the comparison of Fig. 5 with Fig. 6. It is also clear from these plots, that although large anisotropic shear may diminish the number of e-foldings, yet, it never forbids the occurrence of inflation. The right plot in Fig. 6, shows the time evolutions of the number of e-foldings, for  $\dot{\phi}(0) > 0$ , starting with different anisotropy but with the same initial  $\dot{\phi}(0) = 0.1 m_{\text{Pl}}^2$ . It is evident that the maximum number of e-foldings decreases with an increasing initial anisotropy. In Table-I we provide a representative summary for various simulations to determine the number of e-foldings obtained during the inflationary phase for various initial values of the  $\dot{\phi}(0) = (-0.002, 0.002, -0.02, 0.02) m_{\text{Pl}}^2$ , and different values of initial anisotropic shear for  $\phi(0) = (1.0, 2.0, 3.0, 3.14, 4.0, 5.0) m_{\text{Pl}}$ . It is clearly seen that at large anisotropic shear, the number of e-foldings for a given  $\phi(0)$  is almost the same for all  $\dot{\phi}(0)$ .

### 3. Phase portrait and attractor behavior

We now discuss the phase-space trajectories of an inflationary Bianchi-I spacetime in the classical theory. Fig. 7 shows the evolution of various classical trajectories in the  $\phi - \dot{\phi}$  space for Bianchi-I



$\dot{\phi}(0) (m_{\text{Pl}}^2)$	$\epsilon_J^2$	$\phi(0) (m_{\text{Pl}})$					
		1.0	2.0	3.0	3.14	4.0	5.0
-0.002	0	1.551	2.755	20.600	24.195	52.051	96.749
	0.060	1.503	2.849	20.790	24.398	52.326	97.101
	1.084	0.907	4.947	23.587	27.369	57.364	102.195
	$9.665 \times 10^4$	6.388	25.322	56.727	62.122	100.662	157.145
	$5.994 \times 10^8$	6.563	25.646	57.195	62.611	101.271	157.892
	$3.881 \times 10^{19}$	6.566	25.651	57.203	62.619	101.282	157.905
	$1.565 \times 10^{41}$	6.566	25.651	57.203	62.619	101.282	157.905
0.002	0	31.055	62.534	106.206	113.788	161.763	229.467
	0.060	30.853	62.149	105.86	113.429	161.349	228.988
	1.084	28.018	57.415	100.94	108.343	155.451	222.147
	$9.665 \times 10^4$	6.744	25.970	57.6814	63.118	101.903	158.666
	$5.994 \times 10^8$	6.569	25.657	57.211	62.628	101.292	157.918
	$3.881 \times 10^{19}$	6.566	25.651	57.203	62.619	101.282	157.905
	$1.565 \times 10^{41}$	6.566	25.651	57.203	62.619	101.282	157.905
-0.02	0	3.9404	0.199	12.284	15.163	38.690	78.448
	0.060	3.8420	0.194	12.495	15.393	39.027	78.901
	1.084	2.5564	1.692	15.653	20.1637	43.962	85.487
	$9.665 \times 10^4$	6.358	25.261	56.636	62.028	100.541	156.994
	$5.994 \times 10^8$	6.562	25.645	57.194	62.609	101.269	157.89
	$3.881 \times 10^{19}$	6.566	25.651	57.203	62.619	101.282	157.905
	$1.565 \times 10^{41}$	6.566	25.651	57.203	62.619	101.281	157.905
0.02	0	41.544	77.366	125.623	133.832	185.725	258.003
	0.060	41.230	76.781	125.101	133.296	185.102	257.282
	1.084	36.855	69.644	117.725	125.679	176.281	247.045
	$9.665 \times 10^4$	6.776	26.029	57.773	63.214	102.025	158.818
	$5.994 \times 10^8$	6.569	25.657	57.2126	62.6293	101.294	157.92
	$3.881 \times 10^{19}$	6.566	25.651	57.203	62.619	101.282	157.905
	$1.565 \times 10^{41}$	6.566	25.651	57.203	62.619	101.282	157.905

TABLE I: This table summarizes the number of e-folding in the classical Bianchi-I spacetime for various initial values of  $\dot{\phi}(0)$  and  $\phi(0)$ , depending on value of anisotropic shear present in the initial data. Note that for  $\epsilon_J^2 = 0$ , we have not shown the entries corresponding to  $\phi = 3.14 m_{\text{Pl}}$  leading to 60 e-foldings. For the conditions required to obtain 60 e-foldings in the isotropic case, see footnote-6 in Sec.-IIIA.2

spacetime. Trajectories in the same quadrant correspond to different initial anisotropies but with the same initial values of  $\phi$  and  $\dot{\phi}$ , that is, the initial energy density is fixed for all the trajectories and initial shear scalar is varied. The horizontal (red) arrows show the order of decreasing anisotropy. The trajectories with labels ① and ② correspond to the isotropic spacetime (i.e.  $\epsilon_J = 0$ ). Each isotropic curve is composed of two distinct phases. The vertical part (labeled by ①) corresponds to the phase in which there is no slow-roll. The horizontal part (labeled by ②) corresponds to the slow-roll phase in the isotropic case. The black dots on the trajectories denote the point when the accelerated expansion begins. The trajectories in the upper half of the phase space correspond to  $\dot{\phi}(0) > 0$  and the curves in the lower half show the trajectories for  $\dot{\phi}(0) < 0$ . For all the curves, shown in the Fig. 7, initial conditions on the inflaton are kept fixed at  $|\phi| = 3.14 m_{\text{Pl}}$  and  $|\dot{\phi}(0)| = 0.1 m_{\text{Pl}}^2$ , and the anisotropic shear is varied. It is clearly seen from Fig. 7, that all the trajectories corresponding to various initial values of anisotropic shear meet the slow-roll curve in

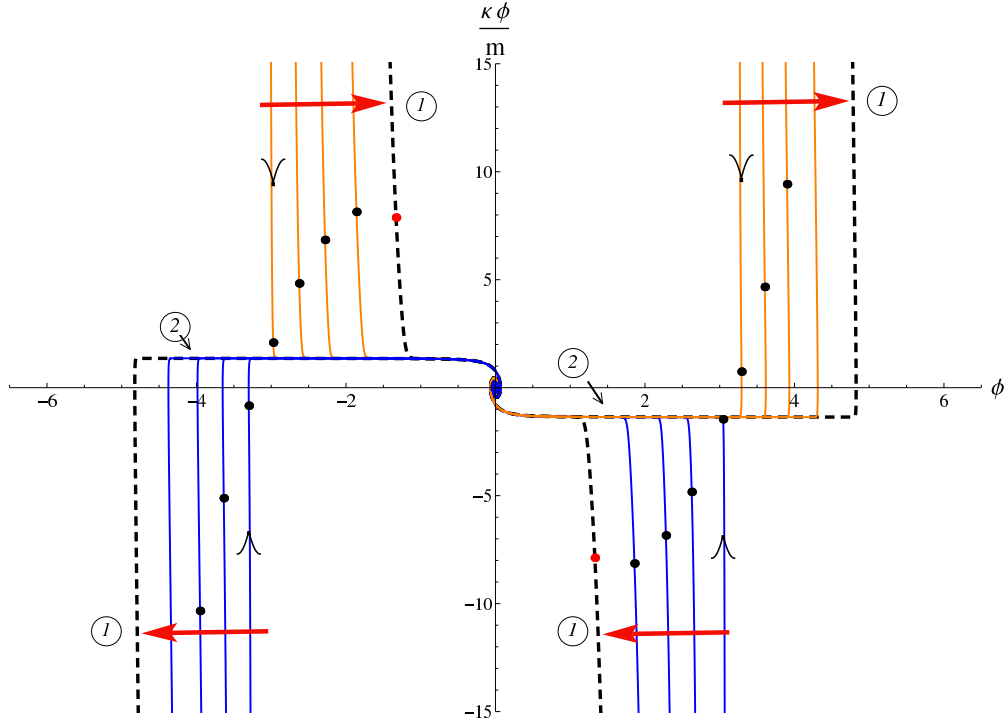


FIG. 7: This figure shows the two attractor behavior of the inflationary Bianchi-I spacetime. The dashed trajectories (denoted by ①) show the isotropic non-slow roll FRW attractor while the horizontal lines to which all the trajectories meet depict the isotropic slow-roll attractor (denoted by ②). The directions of (red) horizontal arrows show decreasing anisotropy (i.e. increasing parameter  $\epsilon_J$ ). The black dots denote the onset of accelerated expansion.  $\kappa$  is  $\kappa = 8\pi G/3$ .

their evolution. In this sense, the isotropic slow-roll is an attractor for all such solutions.

For  $\dot{\phi}(0), \phi(0) > 0$  (also for  $\dot{\phi}(0), \phi(0) < 0$ ), i.e. the initial conditions corresponding to the inflaton rolling up the potential, trajectories in Bianchi-I model remain close to isotropic slow roll curve for a longer time for smaller initial value of the anisotropic shear. Furthermore, with increasing anisotropic shear, the duration of the slow-roll decreases. This behavior is compatible with the variation in the amount of inflation with the varying initial anisotropy discussed earlier. On the other hand, trajectories corresponding to  $\phi(0) > 0$  and  $\dot{\phi}(0) < 0$  (or with  $\phi(0) < 0$  and  $\dot{\phi}(0) > 0$ ) tend to have longer duration of slow-roll for larger value of the anisotropy, which is again compatible with the observation that an increase in anisotropy increases the e-foldings for an inflaton initially rolling down the potential.

Fig. 8 shows the 3D plot of the phase space trajectories of the field in the classical Bianchi-I spacetime. It turns out that as the shear scalar tends to decrease, the phase-space trajectories in classical Bianchi-I spacetime approach that of the corresponding isotropic classical FRW spacetime (with  $\sigma^2 = 0$ ). This behavior is also evident from the Fig. 7 where the thick (red) arrows show the order of decreasing anisotropy. In this sense, in addition to the attraction behavior towards the slow roll trajectory, the non slow roll isotropic curve also acts as an attractor for trajectories in Bianchi-I spacetime in the limit  $\sigma^2 \rightarrow 0$ .<sup>8</sup> In other words, the classical FRW spacetime is an isotropic attractor of the classical Bianchi-I spacetime. That is, as the initial anisotropy is decreased, the trajectories tend closer to the classical FRW isotropic trajectories (shown by the

<sup>8</sup> For an earlier discussion of the second attractor, see Ref. [22].

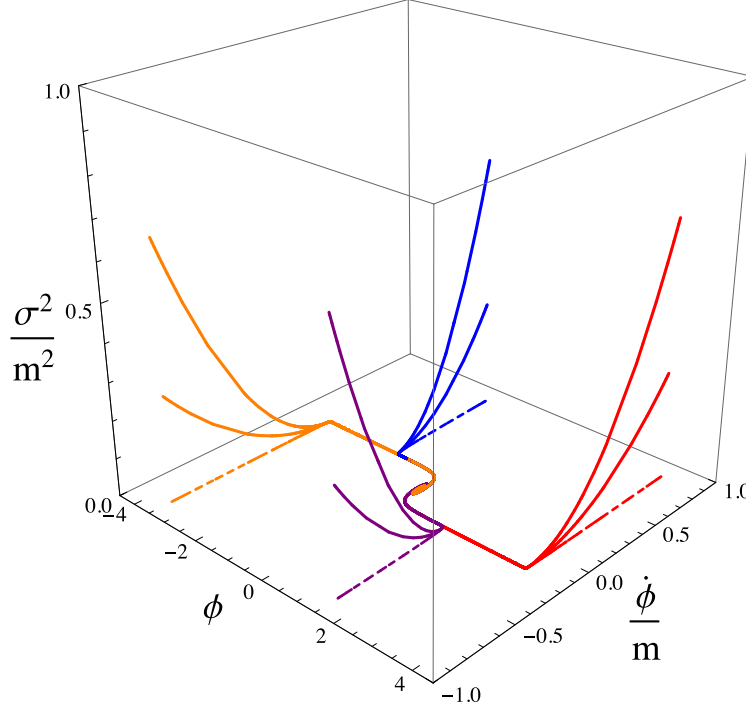


FIG. 8: This figure shows the 3D plot of the phase-space trajectories of the scalar field. The trajectories starting in the same quadrant of  $\phi - \dot{\phi}$  plane correspond to the same initial values of  $\phi$  and  $\dot{\phi}$  but different initial shear scalar. The dashed trajectories in the  $\sigma^2 = 0$  plane depicts the corresponding isotropic trajectories. It is clear that as the shear scalar is decreased the Bianchi-I trajectories tend to the corresponding isotropic trajectory.

dashed-thick lines in Fig. 7 and Fig. 8). To differentiate this attractor from the slow-roll, we call it the ‘non slow-roll FRW attractor’. In this precise sense, there is a double attractor behavior in the classical Bianchi-I spacetime. Before we go into the discussion of numerical results for LQC, a remark about the two attractors is in order.

**Remark:** The two attractors discussed above, namely, the non slow-roll FRW attractor and the isotropic slow-roll attractor, are two distinct properties of the Bianchi-I spacetime. The approach to the isotropic slow-roll is a property of the Bianchi-I spacetime with an inflationary potential. It is achieved in the future evolution when the slow-roll conditions are met, whereas, the non slow-roll FRW attractor can be approached in the pre slow-roll phase of the evolution when the value of the initial anisotropic shear is decreased. In contrast, the slow-roll attractor is approached only after the onset of inflation.

## B. Effective loop quantum dynamics

In this subsection we discuss the results from numerical simulations of the effective dynamical equations of Bianchi-I spacetime in LQC with a  $m^2\phi^2$  potential. The mass of the inflaton is taken to be same as in previous sections:  $m = 1.21 \times 10^{-6} m_{\text{Pl}}$ . Unlike the classical theory, LQC is devoid of initial singularity. The mean scale factor instead of vanishing in the backward evolution, undergoes a non-singular bounce. Hence, LQC provides a way to investigate the inflationary scenario in Bianchi-I spacetime in a non-singular setting. In this article we present the first such study of inflationary Bianchi-I spacetime in a non-singular scenario. The non-singular evolution, in

the effective description of LQC allows us to extend the study of dynamics of Bianchi-I spacetime prior to the onset of inflation, in the deep Planck regime.

As discussed in the previous section, irrespective of the initial conditions, all the curvature invariants of Bianchi-I spacetime are bounded and never diverge during the evolution given by the effective dynamical equations. This implies that the occurrence of bounce is a generic feature of the effective description of Bianchi-I spacetime in LQC, and bounce is obtained without violating any energy condition. If one starts with a classical expanding universe, so that the spacetime curvature is too small for the quantum geometric effects to be important, then during the backward evolution, initially the classical trajectory agrees well with the effective trajectory. In the further backward evolution, as the curvature of spacetime grows, the quantum geometric effects start becoming more prominent. Due to this, the effective trajectory starts deviating from the classical trajectory. In the subsequent backward evolution, the classical trajectory meets the initial singularity, when the mean scale factor goes to zero. On the other hand, the effective trajectory undergoes a smooth non-singular evolution, with the mean scale factor bouncing from a finite non-vanishing value. The individual scale factors, also, undergo smooth evolution from one side of the bounce of the mean scale factor to the other side. Figs. (9(a) and 10(a)) show two examples of evolution of the mean and the directional scale factors of Bianchi-I spacetime in LQC, with initial conditions being provided far from the bounce, close to the onset of inflation. The corresponding evolutions of the energy density and shear scalar are shown in Figs. (9(b, c) and 10(b, c)). The initial conditions for the evolutions shown in Fig. 9 are  $\phi(0) = 3.14 m_{\text{Pl}}$ ,  $\dot{\phi}(0) = -1.97 \times 10^{-7} m_{\text{Pl}}^2$ ,  $\sigma^2(0) = 1.09 \times 10^{-16} l_{\text{Pl}}^{-2}$ , and the initial mean scale factor is  $a(0) = 8.02 \times 10^3$  while the initial energy density being  $\rho(0) = 7.23 \times 10^{-12} m_{\text{Pl}}^4$ . Similarly the initial conditions for the evolution shown in Fig. 10 are  $\phi(0) = 3.14 m_{\text{Pl}}$ ,  $\dot{\phi}(0) = -1.99 \times 10^{-7} m_{\text{Pl}}^2$ ,  $\sigma^2(0) = 9.32 \times 10^{19} l_{\text{Pl}}^{-2}$ ,  $a(0) = 8.05 \times 10^3$  and  $\rho(0) = 7.24 \times 10^{-12} m_{\text{Pl}}^4$ . It is evident from Fig. (9 and 10) that the energy density and the shear scalars do not diverge, and are below their maximum values  $\rho_{\text{max}}$  and  $\sigma_{\text{max}}^2$  throughout the non-singular evolution. The values of the energy density and shear scalar at the bounce can be quite different, as can be seen by comparing Fig. 9 and Fig. 10. It is worth emphasizing that the bounce occurs without any fine tuning of the initial conditions or parameters.

Since the bounce is a generic property of all the solutions in the effective dynamics of LQC, it provides a natural point in the evolution to specify initial data. In all the simulations which we discuss in the following, the initial conditions are provided at the bounce, characterized by  $t = 0$ . The bounce is characterized by the turn around of the mean scale factor which entails vanishing mean Hubble rate,  $H(0) = 0$  at the bounce. Therefore, the initial conditions along with satisfying the Hamiltonian constraint, must be chosen such that the mean Hubble rate equals zero. To ensure this, we provide  $p_1(0)$ ,  $p_2(0)$ ,  $p_3(0)$ ,  $c_1(0)$ ,  $\phi(0)$ , and  $\dot{\phi}(0)$  at the bounce, and compute the value of  $c_2(0)$  and  $c_3(0)$  by requiring that both the Hamiltonian constraint and the mean Hubble rate vanish. Keeping  $p_i(0)$ ,  $\phi(0)$ ,  $\dot{\phi}(0)$  fixed, and by varying  $c_1(0)$  at the bounce, we can vary the initial anisotropic shear scalar at the bounce for a fixed value of the energy density. This gives rise to a continuous set of solutions with a fixed energy density and varying initial shear scalar, all starting at the bounce. These solutions turn out to be the key to understand the effect of varying anisotropic shear scalar on the number of e-foldings. To illustrate, Fig. 11 shows the bounce of mean scale factors for varying  $\sigma^2(0)$  for the same  $\phi(0) = 3.14 m_{\text{Pl}}$  and  $\dot{\phi}(0) = -0.002 m_{\text{Pl}}^2$  at the bounce. As in the previous sections, we choose the initial value of the inflaton field same as above to discuss the qualitative behaviors shown in the plots in this subsection. Results for different initial values of inflaton field will be given in the tabular form (see Table-II). Another way of generating initial conditions with varying initial shear scalar is to vary the initial energy density by varying the initial velocity of the inflaton. This method of choosing initial data is essential in order to understand the isotropic attractor behavior of Bianchi-I spacetime in LQC, as we will see later in this subsection.

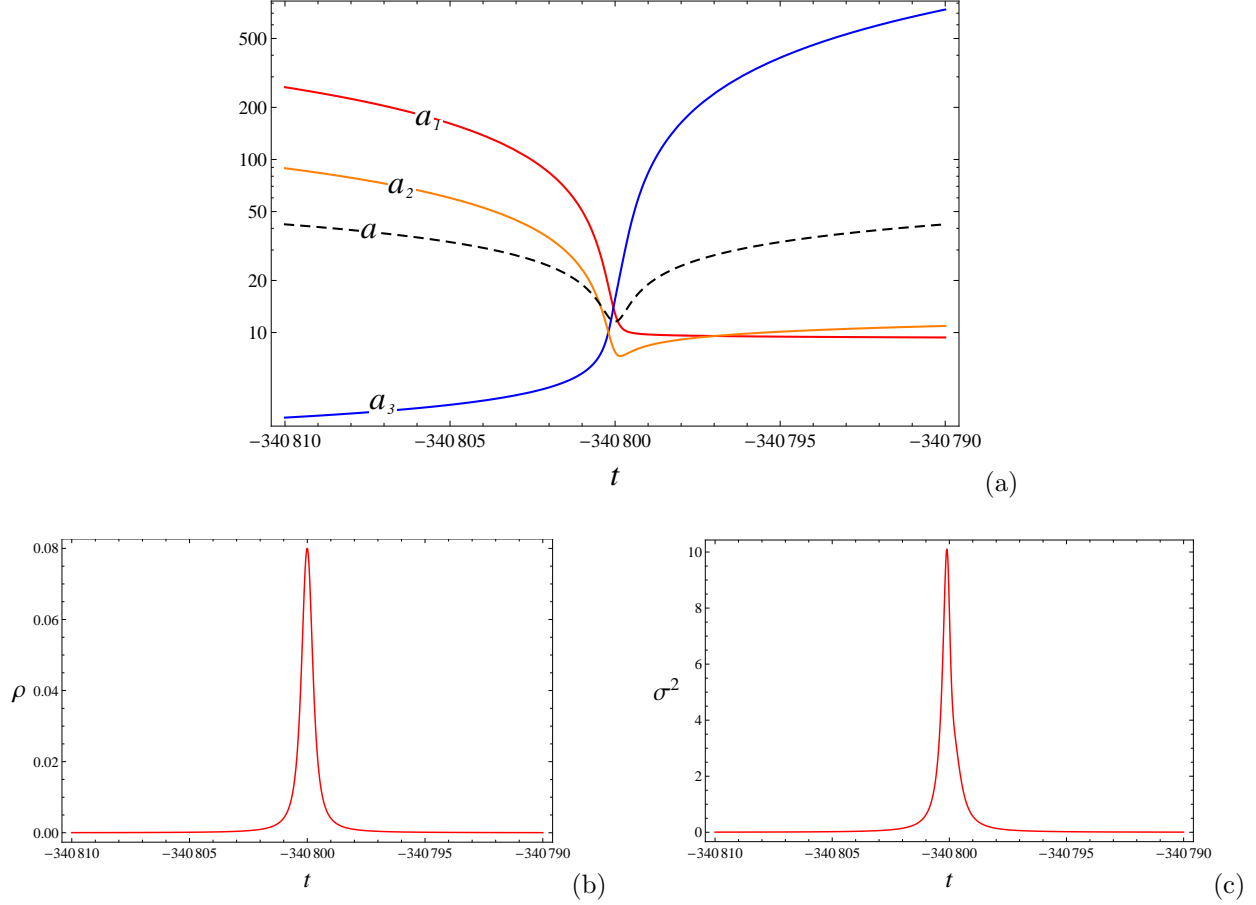


FIG. 9: The figure (a) shows the evolution of the mean and directional scale factors, close to the bounce, when initial conditions are given far from the bounce near the onset of inflation. Figures (b) and (c) show the evolution of energy density and the shear scalar respectively. The values of  $\rho$  and  $\sigma^2$  are in Planck units. The initial conditions for this figure are  $\phi(0) \approx 3.14 m_{\text{Pl}}$ ,  $\dot{\phi}(0) \approx -1.97 \times 10^{-7} m_{\text{Pl}}^2$  and  $\sigma^2(0) \approx 1.09 \times 10^{-16} l_{\text{Pl}}^{-2}$ . It is clear from the plots that the mean scale factor bounces while the directional scale factors undergo smooth evolution.

In the following, we first study the evolution of the individual directional scale factors and the isotropization of Bianchi-I spacetime as the future evolution takes place. Then, we turn to compute the amount of inflation in terms of the number of e-foldings generated during the inflationary era, for a variety of initial conditions including different initial  $\dot{\phi}$ ,  $\phi$  and  $\sigma^2$  at the bounce. We also study the evolution of dynamical trajectories in the  $\phi - \dot{\phi}$  phase space, starting from different initial conditions. The study of the phase trajectories brings out important features of the attractor behavior of Bianchi-I spacetime in effective description of LQC.

### 1. Directional scale factors and isotropization

We study the evolution of the spacetime starting from initial conditions characterized by the presence of a significant anisotropic shear. Due to the non-vanishing anisotropic shear, as in the classical theory, depending on the strength of the anisotropy, the expansion of the spacetime can be highly anisotropic. That is, while the mean scale factor expands, one or two of the directional scale factors decrease and the remaining one(s) increase in the forward evolution. However, in contrast to the classical theory, the backward evolution in LQC is non-singular. Here, we are interested in

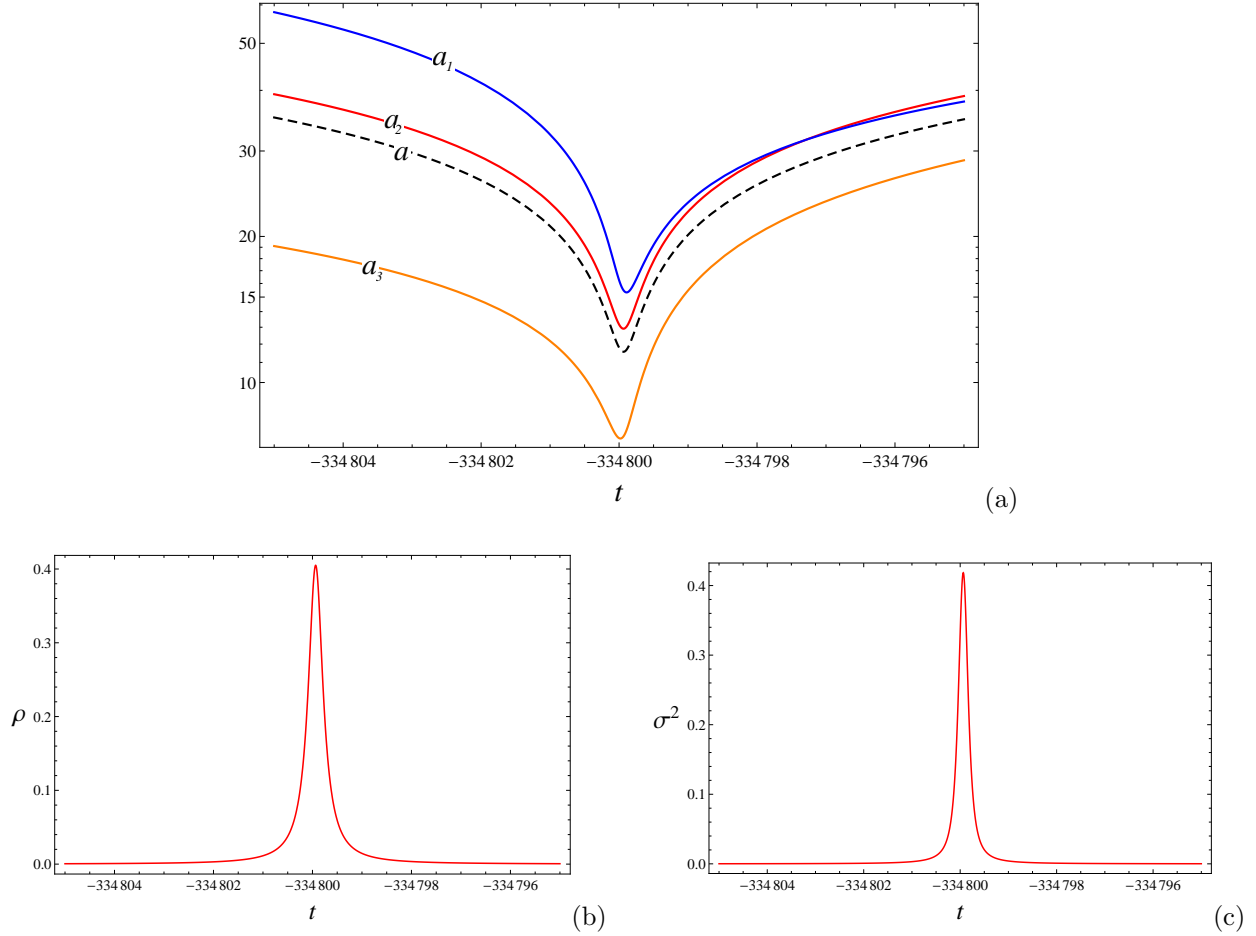


FIG. 10: The figure (a) shows the evolution of the mean and directional scale factors, close to the bounce, when initial conditions are given far from the bounce near the onset of inflation. Figures (b) and (c) show the evolution of energy density and the shear scalar respectively. The values of  $\rho$  and  $\sigma^2$  are in Planck units. The initial conditions for this figure are  $\phi(0) \approx 3.14 m_{\text{Pl}}$ ,  $\dot{\phi}(0) \approx -1.99 \times 10^{-7} m_{\text{Pl}}^2$  and  $\sigma^2(0) = 9.32 \times 10^{-19} l_{\text{Pl}}^{-2}$ . It is clear from the plots that the mean scale factor bounces while the directional scale factors undergo smooth evolution.

investigating the way an anisotropically expanding universe at the bounce turns into isotropically inflating spacetime in LQC.

In Fig. 12, we show the evolution of scale factors in a representative simulation in the Bianchi-I spacetime in LQC. In the expanding branch of the mean scale factor  $a$ , two scale factors are expanding and one is contracting near the bounce. This corresponds to a cigar like structure of the spatial geometry close to the bounce, in the backward evolution of the expanding branch. It turns out that long before the onset of accelerated expansion, LQC trajectory enters into the classical domain, and the shear scalar monotonically falls as  $\sim a^{-6}$ . Due to the ever decreasing shear scalar, in this domain, the parameter  $\epsilon_J$  keeps decreasing and, just like in the classical theory, reaches  $\epsilon_J < 2/\sqrt{3}$  before or right after the onset of inflation. As the accelerated expansion starts to take place, like in the classical theory, the parameter  $\epsilon_J$  falls even more quickly and the contracting directional scale factor turns around, causing isotropization of the Bianchi-I universe in LQC.

In Sec. IIA3, we discussed the evolution of kinetic and potential energies and compared them with the anisotropic shear contribution ( $\sigma^2/16\pi G$ ) in the classical theory. We now study their behavior in LQC. Fig. 13 shows an example of the evolution of all of the three in an expanding

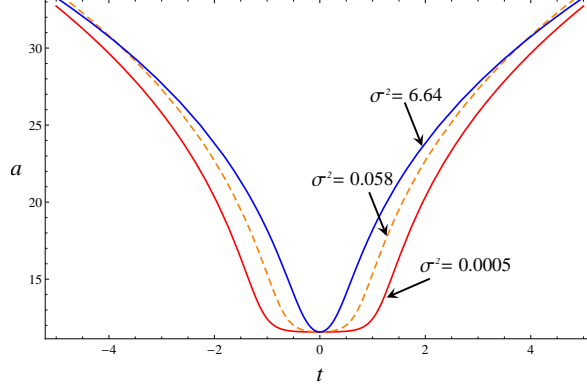


FIG. 11: This figure shows the evolution of the mean scale factor for different initial shear scalars (but with the same initial  $\phi = 3.14 m_{\text{Pl}}$  and  $\dot{\phi} = -0.002 m_{\text{Pl}}^2$ ) given at the bounce. The values of the shear scalar shown in the figure correspond to the values at the bounce (in units of  $l_{\text{Pl}}^{-2}$ ).

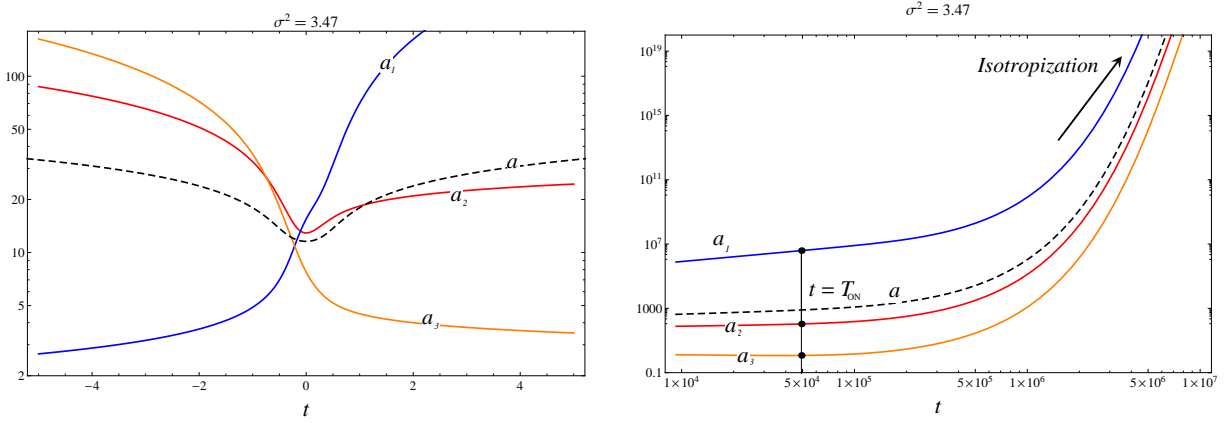


FIG. 12: This figure shows the evolution of directional scale factors for  $\sigma^2(0) = 3.47 l_{\text{Pl}}^{-2}$  at the bounce with initial  $\phi = 3.14 m_{\text{Pl}}$  and  $\dot{\phi} = -0.002 m_{\text{Pl}}^2$ . The right plot shows the isotropization of the directional scale factors. At the bounce one of the scale factors start out in decreasing state but as the inflationary era progresses, all the three directions turn to expand.

branch of inflationary Bianchi-I spacetime. Starting with a shear dominant initial conditions such that kinetic energy dominates over the potential energy, the kinetic energy monotonically decays, whereas, the shear energy shows a non-monotonic behavior in the vicinity of the bounce i.e. it attains a local maximum and then continues to decrease. In the forward evolution, as the spacetime curvature approaches the classical conditions, the anisotropic shear decreases monotonically. This behavior of the anisotropic shear stands in contrast with the classical evolution where the shear term  $\sigma^2$  monotonically decreases in an expanding universe for generic initial conditions. This brings out a key difference between the process of isotropization in classical and LQC evolutions.

It is also clear from the plot that the onset of accelerated expansion (marked by the black dot) takes place when the potential energy wins over the shear and kinetic energy, just like in the classical theory. This is not surprising because, in the above numerical simulation, at the onset of inflation the spacetime is well approximated with a classical solution. Following the start of inflation there may be a period where the contribution of anisotropic shear is still greater than kinetic energy (while contribution of potential energy being larger than the both). However, the shear scalar quickly fades away giving rise to isotropization during the inflationary phase. In this

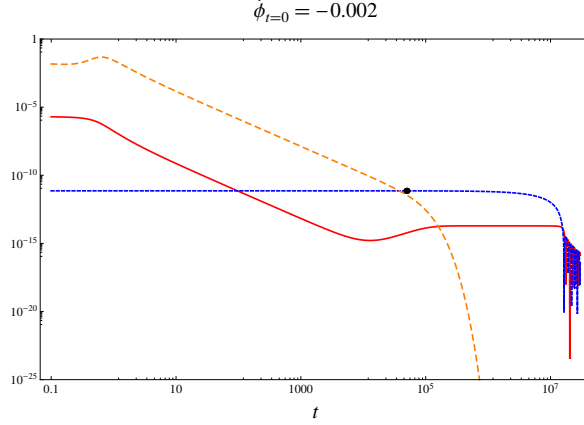


FIG. 13: Evolution of the kinetic ( $\dot{\phi}^2/2$ ), potential ( $m^2\phi^2/2$ ) and anisotropic shear contribution ( $\sigma^2/16\pi G$ ) in LQC effective dynamics. The short dashed (blue) curve represents potential energy, the dashed (orange) line corresponds to the shear contribution and the solid (red) line shows the evolution of kinetic energy of the inflaton.

way, similar to the classical theory, there may be a short period in the inflationary era when the anisotropic shear dominates the kinetic energy, while the potential energy remains greater than both.

## 2. Amount of inflation

We discussed earlier that the amount of inflation in the classical theory increases with increasing initial value of the shear scalar, for an inflaton which is rolling down. Since the shear scalar increases the mean Hubble rate it enhances the damping term in the Klein-Gordon equation. This in turn causes the slow roll conditions to be achieved earlier. Unlike the classical theory, in LQC the mean Hubble rate is not necessarily a monotonic function of the shear scalar. Due to the higher order corrections introduced by the underlying quantum geometry, the modified form of generalized Friedmann equation for Bianchi-I spacetime may contain nonlinear terms<sup>9</sup> in  $\sigma^2$ . Fig. 14 shows the variation of the mean Hubble rate with an increasing initial value of shear scalar. It is evident that the mean Hubble rate shows a non-monotonic behavior with increasing shear scalar, and attains a maximum at some value of  $\sigma^2$ . A result of this is that, in LQC, in the presence of anisotropic shear the number of e-foldings can show a non-monotonic behavior with an increasing shear scalar (while keeping the  $\dot{\phi}(0)$  fixed). Fig. 15 shows the variation of the number of e-foldings for various different values of the initial energy density and  $\dot{\phi}(0) < 0$  at the bounce. It turns out that for small shear scalar, the number of e-foldings ( $N$ ) increases with the values of shear scalar, then  $N$  attains a maximum value at some  $\sigma^2 = \sigma_*^2$ . For any higher value of anisotropic shear than  $\sigma_*^2$ , the amount of e-foldings decreases. Note that, for the values of the parameters considered here, the changes in the number of e-foldings is very small, as can be seen in Fig. 15. In the numerical simulations,  $\sigma_*^2$  turns out to be  $\sigma_*^2 \approx 1.47 l_{\text{Pl}}^{-2}$  for  $|\dot{\phi}(0)| < 0.02 m_{\text{Pl}}^2$ , and for  $|\dot{\phi}(0)| > 0.02 m_{\text{Pl}}^2$  it weakly depends on the initial data. At this point the occurrence of  $\sigma_*^2$  is only a numerical result. Due to the unavailability of the generalized Friedmann equation for Bianchi-I spacetime in LQC, we do not yet have analytical argument to explain its existence.

<sup>9</sup> For example, an approximate expression in the small shear limit, discussed in the Ref. [69], contains  $\sigma^4$  terms with opposite sign to  $\sigma^2$  term, suggesting non-monotonic behavior of the mean Hubble rate with shear scalar.



As in the classical theory, for an opposite sign of  $\dot{\phi}$  in the initial data (in this case the initial data given at the bounce), the amount of inflation shows opposite behavior with the initial anisotropic shear. The numerical simulations performed for  $\dot{\phi}(0) > 0$  are shown in Fig. 16. It is evident that for  $\dot{\phi}(0) > 0$ , in contrast to  $\dot{\phi}(0) < 0$ ,  $N$  decreases with increasing  $\sigma^2$  in the small shear regime, while it increases for  $\sigma^2 > \sigma_*^2$ . Interestingly, the value of  $\sigma_*^2$  turns out to be numerically same as that for  $\dot{\phi}(0) < 0$ .

Such a variation of  $N$  with initial anisotropy is tied to the behavior of the mean Hubble rate. As discussed in the classical theory, an enhancement in the mean Hubble rate, results in an increment in the amount of inflation if the inflaton is initially rolling down, and a decrement if it is rolling up. In LQC, since the mean Hubble rate first increases, attains a maximum and then decreases with increasing initial shear scalar (Fig. 14), the amount of inflation varies in the same way for  $\dot{\phi}(0) < 0$  (Fig. 15). That is, it first increases, attains a maximum and then falls down. The behavior of  $N$  for  $\dot{\phi}(0) > 0$  is opposite to that of  $\dot{\phi}(0) < 0$ .

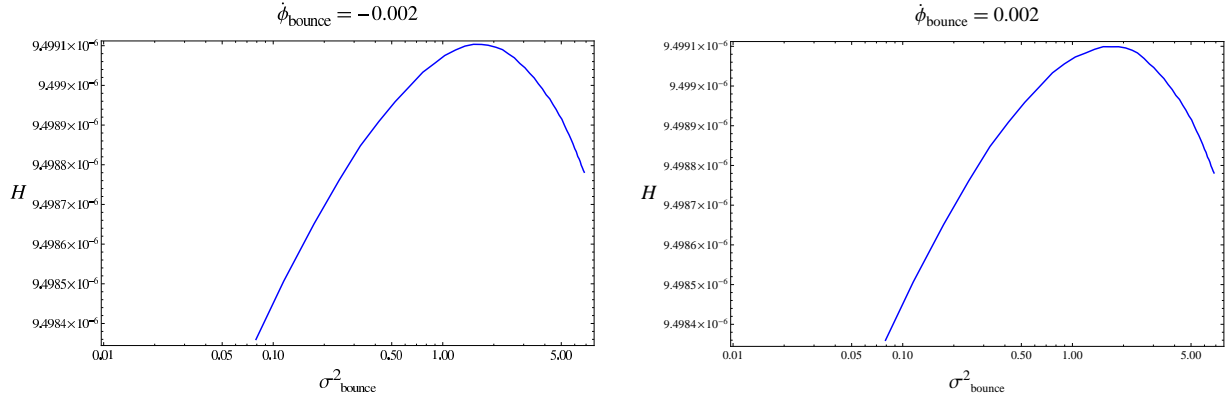


FIG. 14: This figure shows the non-monotonic behavior of the mean Hubble rate at the onset of inflation with varying initial value of the shear scalar at the bounce. The left plot corresponds to a negative initial  $\dot{\phi}$  and the right plot corresponds to a positive initial  $\dot{\phi}$  (in Planck units).

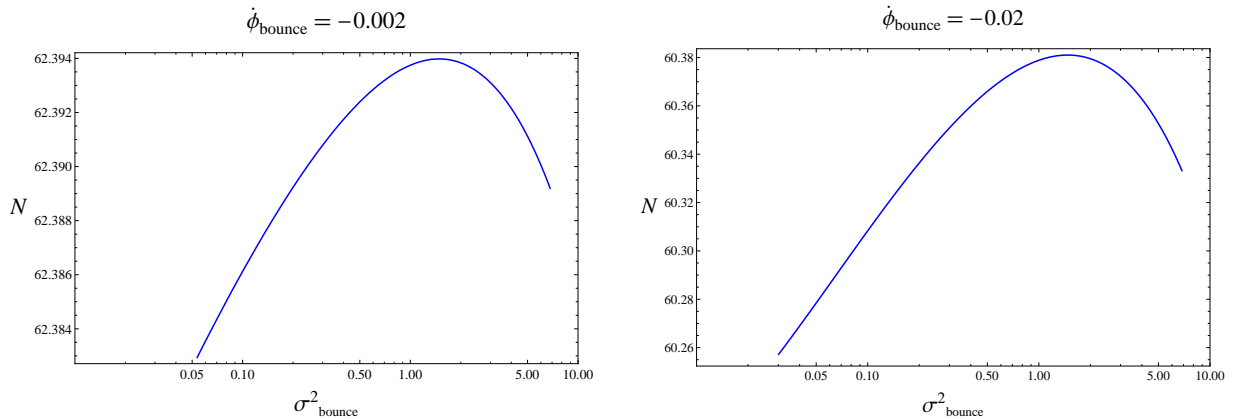


FIG. 15: This figure shows the variation of the number of e-foldings with the changing shear scalar at the bounce for  $\dot{\phi} < 0$  at the bounce. The values of  $\dot{\phi}$  are given in the units of  $m_{\text{Pl}}^2$ .

So far we have discussed the qualitative behavior of the amount of inflation with varying initial anisotropy at the bounce, let us now turn to a more quantitative analysis. An interesting feature of Bianchi-I spacetime lies in the comparison with the isotropic spacetime. It is important to note

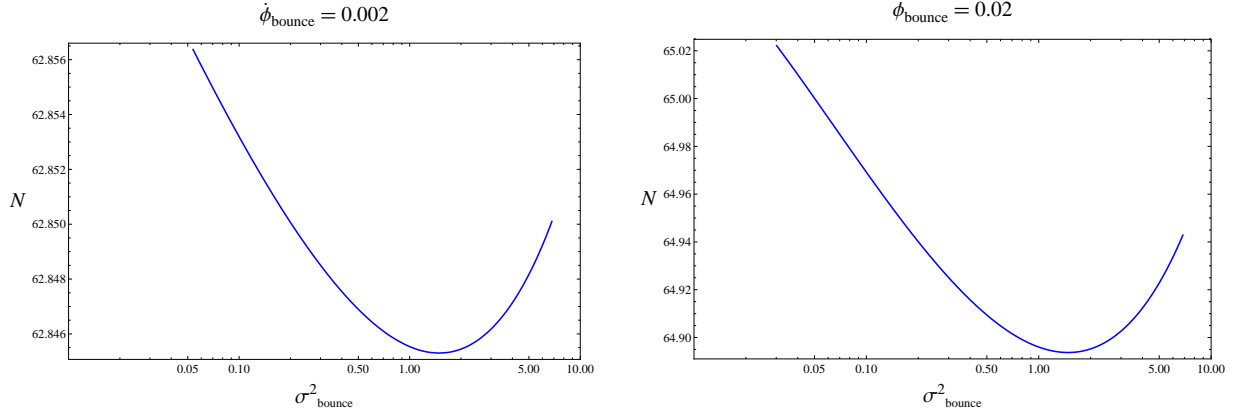


FIG. 16: Variation of the number of e-foldings with the changing shear scalar at the bounce for  $\dot{\phi} > 0$  at the bounce. The values of  $\dot{\phi}$  and  $\sigma^2$  are in the units of  $m_{\text{Pl}}^2$  and  $l_{\text{Pl}}^{-2}$  respectively.

that in the isotropic spacetime, if  $\phi(0) = 3.14m_{\text{Pl}}$  at the bounce then the value of  $\dot{\phi}$  at the bounce is fixed to  $|\dot{\phi}(0)| \approx 0.905m_{\text{Pl}}^2$  as the bounce always occurs when energy density saturates its upper maximum  $\rho = \rho_{\text{max}} = 0.41\rho_{\text{Pl}}$ . Whereas, in the Bianchi-I spacetime, since the energy density may not be saturated at the bounce,  $|\dot{\phi}(0)| < 0.905m_{\text{Pl}}^2$  is allowed. In this way, there is a freedom in the choice of initial inflaton velocity at the bounce in Bianchi-I spacetime, as compared to the isotropic spacetime. Table-II shows the number of e-foldings for various initial values of the inflaton field with  $\phi(0) = (1.0, 2.0, 3.0, 3.14, 4.0, 5.0)m_{\text{Pl}}$ . For each of  $\phi(0)$ , as we just discussed, there are several possible initial  $\dot{\phi}$  in the Bianchi-I spacetime, unlike in the isotropic spacetime where the inflaton velocity at the bounce is fixed for a given  $\phi(0)$ . This table shows the number of e-foldings for different initial velocities  $\dot{\phi}(0) = (-0.002, 0.002, -0.02, 0.02)m_{\text{Pl}}^2$  with varying initial shear scalar for each of the  $\phi(0)$  given at the bounce. The last two rows of Table - II with  $|\dot{\phi}(0)| = 0.905m_{\text{Pl}}^2$  correspond to the isotropic spacetime, characterized by  $\sigma^2(0) = 0$ . It is evident from the analysis of Table-II that, if the inflaton is initially rolling down, then, the Bianchi-I spacetime can produce significantly more number of e-foldings than in the isotropic spacetime. For example, if the initial value of inflaton field is  $\phi(0) = 3.14m_{\text{Pl}}$  then the number of e-foldings in Bianchi-I spacetime is of the order of 60 while for the same initial value of inflaton the isotropic spacetime produces e-foldings as small as 3.103, if the inflaton is initially rolling down. In the same way, the maximum number of e-foldings for  $\phi(0) = 3.0m_{\text{Pl}}$  in Bianchi-I spacetime is of the order of 50 compared to the isotropic spacetime where  $N \approx 1.648$ . In order to generate  $N \approx 60$ , in the isotropic spacetime for an inflaton initially rolling down, the initial value of the inflaton should be  $\phi(0) \approx 5.50m_{\text{Pl}}$  whereas, the same amount of e-foldings can be generated in the Bianchi-I spacetime for a lower initial value of inflaton  $\phi(0) < 5.50m_{\text{Pl}}$  (see Table-II). In this way, presence of anisotropy widens up the window of the values of the initial inflaton field, at the bounce, which produces a given amount of inflation.

### 3. Phase portrait and attractor behavior

Let us now explore the properties of the dynamical trajectories in LQC. We will discuss the trajectories of both the matter and the gravitational sector i.e.  $(\phi, \dot{\phi})$  for the inflaton and  $(\log(a), H)$  for the gravitational part respectively. A phase portrait of Bianchi-I spacetime in LQC is shown in Fig. 17. The left plot corresponds to the inflaton in which the dashed thick lines show the isotropic trajectories with the initial conditions  $\phi(0) = \pm 3.14m_{\text{Pl}}$  and  $\dot{\phi}(0) \approx \pm 0.905m_{\text{Pl}}^2$  at the bounce. The

Number of e-foldings							
$\dot{\phi}(0)(m_{\text{Pl}}^2)$	$\sigma^2(0)(l_{\text{Pl}}^{-2})$	$\phi(0) (m_{\text{Pl}})$					
		1.0	2.0	3.0	3.14	4.0	5.0
-0.002	0.002	6.477	23.548	56.959	62.404	101.016	155.575
	0.277	6.486	23.555	56.971	62.426	101.03	155.592
	0.967	6.486	23.559	56.976	62.428	101.037	155.601
	1.441	6.487	23.561	56.979	62.429	101.041	155.606
	3.184	6.486	23.562	56.981	62.428	101.044	155.61
	5.983	6.485	23.563	56.983	62.425	101.046	155.613
	6.831	6.484	23.564	56.984	62.424	101.048	155.615
0.002	0.002	6.654	23.887	57.447	62.833	101.659	156.365
	0.277	6.645	23.880	57.436	62.812	101.645	156.347
	0.967	6.644	23.877	57.431	62.809	101.638	156.339
	1.441	6.644	23.874	57.427	62.809	101.633	156.333
	3.184	6.645	23.873	57.425	62.811	101.63	156.33
	5.983	6.646	23.872	57.424	62.812	101.628	156.327
	6.831	6.647	23.871	57.423	62.813	101.627	156.325
-0.02	0.049	5.765	23.548	56.959	60.278	101.016	155.575
	0.287	5.787	23.555	56.970	60.352	101.03	155.592
	0.976	5.795	23.559	56.975	60.377	101.037	155.601
	1.450	5.795	23.561	56.978	60.381	101.041	155.606
	3.194	5.789	23.562	56.981	60.361	101.044	155.61
	5.993	5.779	23.563	56.982	60.349	101.046	155.613
	6.841	5.776	23.564	56.983	60.333	101.048	155.615
0.02	0.049	7.409	27.221	59.486	65.001	105.226	161.673
	0.287	7.385	27.233	59.502	64.924	105.248	161.700
	0.976	7.376	27.217	59.479	64.898	105.218	161.663
	1.450	7.376	27.203	59.457	64.893	105.188	161.626
	3.194	7.382	27.191	59.439	64.915	105.164	161.596
	5.993	7.394	27.182	59.425	64.924	105.145	161.572
	6.841	7.397	27.175	59.415	64.943	105.131	161.554
-0.905	<b>0</b>	12.595	2.087	1.648	3.103	17.997	47.994
0.905	<b>0</b>	66.835	111.65	168.524	177.454	237.553	318.805

TABLE II: This table summarizes the variation of number of e-foldings with varying shear scalar at the bounce, for various initial  $\dot{\phi}$  at the bounce.

solid (blue) curve and the dotted-dashed (red) curves correspond to the LQC trajectories with the initial conditions at the bounce as  $\phi(0) = \pm 3.14 m_{\text{Pl}}$  and  $\dot{\phi}(0) = \pm 0.002 m_{\text{Pl}}^2$ . In this phase portrait, the first and third quadrant correspond to an inflaton which is initially rolling up, while the second and fourth quadrant represent the trajectories when the inflaton is rolling down the potential. The slow-roll is characterized by the horizontal line, with an almost constant  $\dot{\phi}$ , to which all the trajectories meet in their future evolution. It is evident that for a rolling down inflaton with the given initial conditions, the Bianchi-I trajectory remains on the slow-roll curve for a longer period of evolution than the isotropic trajectory. In this way, the presence of anisotropic shear at the bounce (even a small value) leads the dynamical trajectory to meet the slow-roll curve sufficiently early which, in contrast to the isotropic case, results in higher number of e-foldings if the inflaton is initially rolling down the potential.

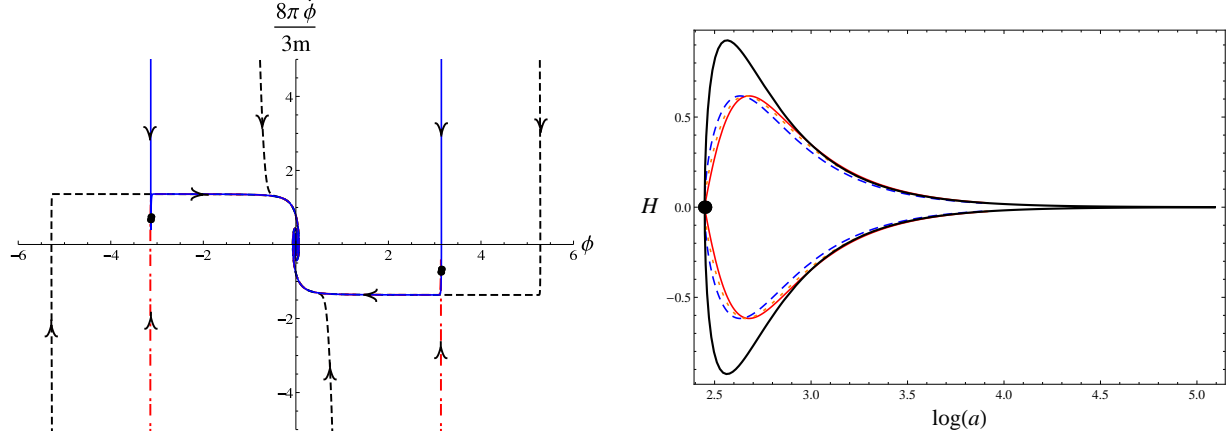


FIG. 17: The left figure shows the phase-space trajectory of the scalar field and the right plot is the plot of the trajectory in the gravitational phase-space  $(\log(a), H)$ .

Analysis of the phase-space trajectories of gravitational variables  $\log(a)$  *vs.*  $H$  gives information about the isotropization of the spacetime. The right plot in Fig. 17 shows the comparison of isotropic trajectories with Bianchi-I trajectories for various values of initial shear at the bounce. The thick (black) curve shows the isotropic trajectory, the dashed (blue) curve corresponds to Bianchi-I trajectory with initial shear scalar  $\sigma^2(0) = 5 \times 10^{-4} l_{\text{Pl}}^{-2}$ , the dashed (orange) curve with initial shear  $\sigma^2(0) = 5.7 \times 10^{-2} l_{\text{Pl}}^{-2}$  and the solid (red) line with  $\sigma^2(0) = 6.81 l_{\text{Pl}}^{-2}$  at the bounce, while the initial conditions on the inflaton are being fixed at  $\dot{\phi}(0) = -0.002 m_{\text{Pl}}^2$  and  $\phi(0) = 3.14 m_{\text{Pl}}$ . The black dot denotes the bounce point of the mean scale factor. It is clear from the plot that, close to the bounce, the evolution of Bianchi-I spacetime trajectories are different from that of the isotropic spacetime. Whereas, away from the bounce when the curvature is much smaller, then all the trajectories tend to meet the isotropic trajectory, leading the spacetime to isotropize.

We now discuss, in detail, a feature of the attractor behavior of Bianchi-I spacetime in the effective description of LQC. Fig. 18 shows the evolution of trajectories starting with the same initial  $\phi(0) = 3.14 m_{\text{Pl}}$  but different initial  $\dot{\phi}$ . For clarity, we only show the first and the fourth quadrant of the phase portrait. The initial values of  $\dot{\phi}$  for the trajectories in the fourth quadrant are  $\dot{\phi}(0) = (-0.905, -0.856, -0.727, -0.584, -0.536, -0.407, -0.289, -0.171, -0.053) m_{\text{Pl}}^2$ , and in the first quadrant,  $\dot{\phi}(0) = (0.0, 0.053, 0.171, 0.289, 0.407, 0.536, 0.584, 0.727, 0.856, 0.905) m_{\text{Pl}}^2$ . The left most trajectory, in the fourth quadrant, denoted by  $\sigma^2 = 0$  corresponds to the isotropic spacetime with  $\dot{\phi}(0) = -0.905 m_{\text{Pl}}^2$ , and the right most trajectory in the first quadrant marked with  $\sigma^2 = 0$  represents the evolution of isotropic spacetime with  $\dot{\phi}(0) = 0.905 m_{\text{Pl}}^2$ . All the other trajectories correspond to Bianchi-I spacetime with non-zero initial anisotropic shear scalar. Recall that in the effective description of Bianchi-I spacetime the shear scalar has an upper bound,  $\sigma_{\text{max}}^2 = 11.57 l_{\text{Pl}}^{-2}$ . Evolution of trajectories starting with initial  $\sigma^2 = \sigma_{\text{max}}^2$  are shown by solid (orange) curves denoted by “ $\sigma^2 = 11.57$ ”. All the other Bianchi-I trajectories correspond to smaller values of initial shear scalar the bounce. The slow-roll curve is characterized by the horizontal line with an almost constant  $\dot{\phi} \approx 1.97 \times 10^{-7} m_{\text{Pl}}^2$ , to which all the trajectories with various initial  $\dot{\phi}(0)$  and  $\sigma^2(0)$  meet in their future evolution. Thus, like in the classical theory, the slow-roll curve turns out to be an attractor for all the trajectories shown in the phase portrait. This implies that irrespective of the initial anisotropic content of the spacetime, all the Bianchi-I spacetime trajectories in the effective description of LQC do meet the slow-roll curve in their future evolution, if the initial  $\phi(0)$  is kept high enough. Thus, we conclude that the presence of non-vanishing anisotropic shear does not prevent the occurrence of slow-roll inflation with  $\phi^2$  potential in Bianchi-I LQC.

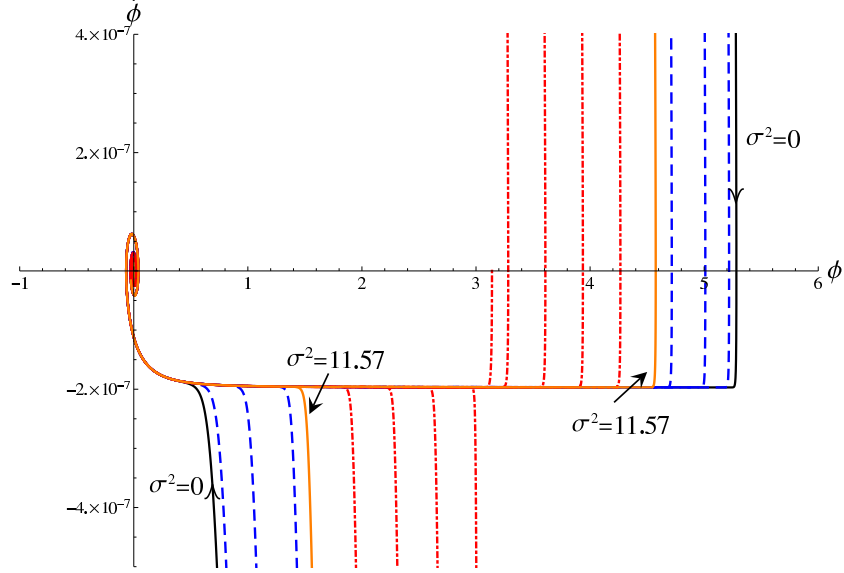


FIG. 18: This figure shows the evolution of various trajectories starting with different  $\dot{\phi}(0) = (-0.905, -0.856, -0.727, -0.584, -0.536, -0.407, -0.289, -0.171, -0.053)m_{\text{Pl}}^2$  starting in the fourth quadrant and  $\dot{\phi}(0) = (0.0, 0.053, 0.171, 0.289, 0.407, 0.536, 0.584, 0.727, 0.856, 0.905)m_{\text{Pl}}^2$  in the first quadrant (from left to right). The solid black curves marked with  $\sigma^2 = 0$  correspond to the isotropic trajectories and the solid (orange) curves denoted by  $\sigma^2 = 11.57$  (in Planck units) correspond to trajectories with maximum shear scalar at the bounce. For all the trajectories, the initial value of the inflaton is kept fixed at  $\phi(0) = 3.14 m_{\text{Pl}}$ . All the values shown in this plot are in Planck units.

In the effective description of LQC, the isotropic spacetime is characterized by two conditions: the first condition requires the vanishing of the shear scalar  $\sigma^2 = 0$  at all times and the second condition requires the energy density to be  $\rho = \rho_{\text{max}}$  at the bounce. This leads to an interesting feature of effective dynamical trajectories of Bianchi-I spacetime regarding its isotropic limit. That is, in order to approach the isotropic limit of Bianchi-I spacetime in effective dynamics of LQC, the energy density at the bounce must tend to approach its maximum, i.e.  $\rho \rightarrow \rho_{\text{max}}$  ( $|\dot{\phi}(0)| \rightarrow 0.905 m_{\text{Pl}}^2$ , if  $\phi(0) = 3.14 m_{\text{Pl}}$ ), along with the shear scalar vanishing, i.e.  $\sigma^2(0) \rightarrow 0$  at the bounce. This stands in contrast with the classical theory, where  $\sigma^2 \rightarrow 0$  is sufficient for Bianchi-I spacetime to approach the isotropic limit, irrespective of the value of the energy density. As discussed earlier, in the classical theory, for a fixed initial energy density, the isotropic limit can be approached by continuously varying the initial  $\sigma^2$  to zero as shown in Fig. 7. Thus, there is an isotropic trajectory corresponding to every initial energy density in the classical theory. In contrast, in LQC, the energy density for an isotropic spacetime must be  $\rho = \rho_{\text{max}}$  at the bounce. In this way, for a given initial value of the inflaton field, there are several classical isotropic trajectories, but there are only two isotropic LQC trajectories (as shown in Fig. 18). These two trajectories correspond to different signs of initial  $\dot{\phi}$ , such that  $\rho = \rho_{\text{max}}$  at the bounce. Therefore, for a given initial value of the inflaton field, there is a unique isotropic curve in each quadrant of the  $\phi - \dot{\phi}$  phase portrait of Bianchi-I spacetime in effective description of LQC. The two isotropic curves corresponding to  $\phi(0) = 3.14 m_{\text{Pl}}$  are shown in Fig. 18, one in first and the other in the fourth quadrant. Starting from any given trajectory in Fig. 18, if one decreases  $\dot{\phi}(0)$  to  $-0.905 m_{\text{Pl}}^2$ , which is the value of  $\dot{\phi}$  at the bounce in the isotropic spacetime for an inflaton which is rolling down, then the Bianchi-I trajectories approach towards the isotropic trajectory in the fourth quadrant. While if one increases  $\dot{\phi}(0)$  to  $0.905 m_{\text{Pl}}^2$ , the value of  $\dot{\phi}$  at the bounce in the isotropic spacetime for an inflaton which is rolling up, then the isotropic trajectory in the first quadrant is approached. In this way, the

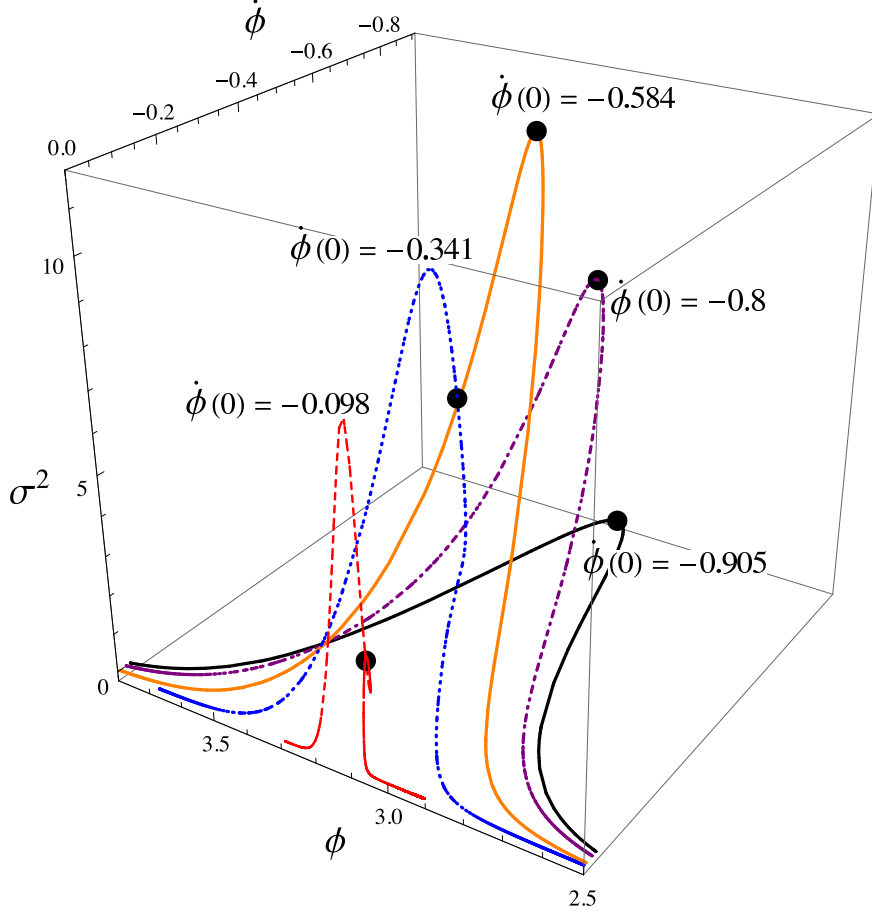


FIG. 19: This plot shows the 3D phase portrait of various trajectories starting with different  $\dot{\phi}(0) < 0$  in the near bounce region. The black dot marks the bounce point. The solid (orange) line corresponds to the maximum shear scalar at the bounce  $\sigma^2 = \sigma_{\text{max}}^2 = 11.57 l_{\text{Pl}}^{-2}$ . The thick black line in the  $\sigma^2 = 0$  plane corresponds to the isotropic trajectory. Clearly, as the value of initial  $\dot{\phi}$  tends to  $-0.905 m_{\text{Pl}}^2$ , the Bianchi-I trajectories approach the isotropic trajectory.

isotropic spacetime turns out to be an “isotropic attractor” of Bianchi-I spacetime in the effective description of LQC. This behavior is easy to understand from a 3D plot of the phase trajectories as shown in Fig. 19, where we show the evolution of Bianchi-I trajectory in the vicinity of the bounce. The solid black trajectory in the  $\sigma^2 = 0$  plane corresponds to the isotropic spacetime with  $\dot{\phi}(0) = -0.905 m_{\text{Pl}}^2$  and all the other ones correspond to Bianchi-I spacetime with different initial  $\dot{\phi}$  and  $\sigma^2$  at the bounce. It is clear to see from this figure that as  $\dot{\phi}(0) \rightarrow -0.905 m_{\text{Pl}}^2$ , the trajectories tend to approach the isotropic trajectory in the  $\sigma^2 = 0$  plane.

It is important to note that the isotropic attractor behavior in LQC is obtained by varying both the initial energy density at the bounce and the shear scalar, whereas in the classical theory the isotropic spacetime can be approached for any fixed initial energy density. If one fixes the energy density, at the bounce in LQC, to any other value than  $\rho_{\text{max}}$  by specifying  $\phi(0)$  and  $\dot{\phi}(0)$  and tries to vary the shear scalar, then it turns out that the shear scalar can not be varied to a value less than a non-zero minimum value which depends on the energy density at the bounce. In this way, again, unless the energy density at the bounce tends to  $\rho_{\text{max}}$ , Bianchi-I trajectories do not approach the isotropic spacetime. Thus, in LQC, isotropic attractor is not obtained for those Bianchi-I trajectories for which  $\rho \neq \rho_{\text{max}}$  at the bounce.

To obtain a complete set of initial data, for the trajectories in Fig. 18, we give  $p_i(0)$ ,  $c_1(0)$ ,  $\phi(0)$

for varying  $\dot{\phi}(0)$ , and the values of  $c_2(0)$ ,  $c_3(0)$  are computed by solving the Hamiltonian constraint and the mean Hubble rate being,  $H = 0$  at the bounce. In the numerical simulations, it turns out that for a fixed value of  $c_1(0)$ , there is a fixed range of the values of  $\dot{\phi}(0)$  for which the Hamiltonian constraint is satisfied. That is,  $\dot{\phi}(0)$  can not be continuously varied from  $-0.905 m_{\text{Pl}}^2$  to  $0.905 m_{\text{Pl}}^2$  for a fixed value of  $c_1(0)$ , in the numerical simulations performed. In this way, depending on various fixed values of  $c_1(0)$ , one can generate a continuous family of trajectories by varying  $\dot{\phi}(0)$  within the corresponding range, which depends on the value  $c_1(0)$ . In each of these ranges, there will be a limiting curve with minimum shear scalar to which the other trajectories in the range tend, as the shear scalar in the initial data decreases. For the simulations shown in Fig. 18, one has to choose atleast two different values of  $c_1(0)$ , one for  $|\dot{\phi}(0)| < 0.5839 m_{\text{Pl}}^2$  and another for  $|\dot{\phi}(0)| > 0.5839 m_{\text{Pl}}^2$ .

It is now clear from the discussion of the phase portraits of the inflationary Bianchi-I spacetime that:

- Trajectories starting with a wide variety of initial conditions meet the slow-roll trajectory in the future evolution. This indicates slow-roll is an attractor for Bianchi-I spacetime.
- Isotropic spacetime behaves like an “isotropic attractor” for Bianchi-I spacetime if the isotropic limit is taken by considering both  $\sigma^2(0) \rightarrow 0$  and  $\rho(0) \rightarrow \rho_{\text{max}}$  at the bounce. For the trajectories, for which the initial energy density does not approach  $\rho_{\text{max}}$  at the bounce, the isotropic limit does not exist.

Hence, the two attractor behavior present in the classical Bianchi-I spacetime with  $\phi^2$  potential, is also present in the effective description of LQC, with the above noted subtlety in the way isotropic limit of Bianchi-I spacetime is taken. It is worth emphasizing that due to quantum geometric effects in the pre-inflationary era, the physical trajectories of the effective description are very different from those of the classical Bianchi-I spacetime. It is due to these differences that the conditions to approach the isotropic limit are modified in the effective description of LQC as compared to the classical theory.

#### IV. DISCUSSION

Though the inflationary paradigm has been successful in explaining the physics of the early universe, it is incomplete without understanding the way the initial singularity is resolved and the way inflation begins from generic initial conditions. In this work, we have analyzed these questions for the  $\phi^2$  inflation in the setting of an anisotropic spacetime described by the Bianchi-I model using the effective spacetime approach of LQC and made a comparative analysis with the classical theory. The underlying quantum geometric effects originating from LQG result in a non-singular evolution. The backward evolution in LQC is devoid of the big bang singularity. The latter is replaced by a bounce of the mean scale factor when the spacetime curvature becomes Planckian. The energy density and the shear scalar remain bounded throughout the evolution in LQC. To our knowledge, this is the first such study of the inflationary scenario in Bianchi-I spacetime in a non-singular setting.

One of the key questions in the study of the evolution of the universe is its isotropization from a generic anisotropic universe in the pre-inflationary era. Previous studies of Bianchi-I inflation in the classical theory and brane world cosmology established that the presence of anisotropy does not prevent inflation, and it is actually conducive to the number of e-foldings obtained during the inflationary phase. These studies for quadratic potential took the initial velocity of the inflaton to be negative (i.e. the inflaton initially rolling down the potential). It was found that the amount of

inflation for such initial conditions always increased with increasing shear in the classical theory as well as in brane-world scenarios [20]. We revisited the analysis in the classical theory by taking a more generic initial data by including the case when inflaton is initially rolling up the potential. In this case, we found that in comparison to the corresponding isotropic evolution, the amount of inflation actually decreases with an increasing anisotropic shear. This happens because of the greater anisotropy, the Hubble friction in the Klein-Gordon equation increases which turns up the decay of kinetic energy of the inflaton. Due to the faster decay of the kinetic energy, an inflaton which is initially rolling up, stops at a lower value of the potential which decreases the amount of e-foldings in the subsequent slow-roll evolution. It is worth emphasizing again that the presence of anisotropic shear does *not* rule out inflation. We showed that for accelerated expansion to take place, the potential energy must win over the kinetic and the shear energy. Owing to this property, in the inflationary era, shear term is always less than the potential energy. There may however be, a small period during the accelerated expansion when anisotropic shear contribution ( $\sigma^2/16\pi G$ ) while being less than potential term ( $V(\phi)$ ), is still greater than the kinetic term ( $\dot{\phi}^2/2$ ). In this sense there may be a brief duration of shear dominance in the inflationary phase of Bianchi-I spacetime. We also showed by explicit simulations that if one starts with highly anisotropic initial conditions such that two of the scale factors are contracting and third one is expanding, in the inflationary phase all of the scale factors expand. This property can be attributed to the value of the anisotropy parameter  $\epsilon_J$  which always decreases in an expanding universe. Therefore, irrespective of large initial  $\epsilon_J$ , the shear scalar decreases and due to the accelerated expansion there is a point, in the future evolution, where  $\epsilon_J < 2/\sqrt{3}$  which corresponds to all expanding directions of the Bianchi-I spacetime. Hence, isotropization is inevitable in an inflating classical Bianchi-I spacetime with a  $\phi^2$  potential.

In the analysis of the loop quantum effective dynamics of the inflating Bianchi-I spacetime, the quantum gravitational corrections come into play in the near bounce phase in the pre-inflationary era. Due to the presence of an upper bound on the anisotropic shear and the energy density, the set of initial conditions are quite different from those in the classical theory. Also, to give initial conditions on the bounce point, along with satisfying the Hamiltonian constraint, one has to make sure that the mean Hubble rate is zero, a condition which was not present in the classical theory. Our analysis shows that the amount of inflation in LQC does not change monotonically with the initial anisotropic shear at the bounce. It has a turning point at  $\sigma_*^2$  whose value depends on the initial value of inflaton and its velocity (but is independent of the sign of the initial velocity). For an inflaton initially rolling down the potential, the number of e-foldings increase with anisotropy only when initial  $\sigma^2$  is less than  $\sigma_*^2$ . On the other hand, if the inflaton is initially rolling up, then the number of e-foldings decrease with anisotropy only when initial  $\sigma^2$  is less than  $\sigma_*^2$ . As in the classical theory, isotropization is inevitable in the inflationary LQC Bianchi-I spacetime starting from arbitrary anisotropic initial conditions.

Analysis of the phase space trajectories demonstrate that there is a double attractor behavior in effective dynamics of LQC for Bianchi-I spacetime as in the classical theory, however one has to be careful in taking the isotropic limit at the bounce. In the classical theory, phase space trajectories approach the slow-roll attractor in the future evolution. This holds true also in LQC. There is also a non slow-roll isotropic attractor which is reached by taking the limit  $\sigma^2 \rightarrow 0$  for any value of energy density in the classical theory. In LQC, since energy density is saturated to its universal maximum value  $\rho_{\text{max}}$  at the bounce, the second attractor is reached only for those trajectories starting at the bounce which satisfy  $\sigma^2 \rightarrow 0$  along with  $\rho \rightarrow \rho_{\text{max}}$ .

We conclude our discussion by pointing out that in the Bianchi-I spacetime sufficient number of e-foldings can be obtained by starting at a significantly lower value of the inflaton field at the bounce than in the isotropic LQC when the inflaton is initially rolling down the potential. Further there is more freedom in specifying the initial data at the bounce in the anisotropic model. This can



be of significance in the study of observational signatures of quantum gravitational effects in the pre-inflationary stage of LQC. As an example, it has been recently suggested that for the isotropic LQC, a narrow window depending on the value of the inflaton field at the bounce exists for which there can be potentially distinct signatures of LQC in the cosmic microwave background [72, 73]. Our analysis suggests that such a window potentially widens in the presence of anisotropies if the inflaton is initially rolling down in the pre-inflationary epoch. Owing to widening the window of the value of the inflaton field in Bianchi-I spacetime for the same number of e-foldings in the isotropic case, there could be potentially additional corrections which will again be of quantum gravitational in origin. A complete quantum treatment of the field perturbations in Bianchi-I anisotropic background is expected to bring out additional possible observational signatures of loop quantum effects in the primordial power spectrum.

### Acknowledgments

We thank Abhay Ashtekar, Jacobo Diaz-Polo, Jorge Pullin and Edward Wilson-Ewing for useful discussions and suggestions. This work is supported by NSF grant PHYS1068743 and a grant by the John Templeton Foundation. The opinions expressed in this publication are those of the authors and do not necessarily reflect the views of the John Templeton Foundation. BG's research is partially supported by the Coates Scholar Research Award of Louisiana State University.

- 
- [1] A. Borde, A. H. Guth and A. Vilenkin, Phys. Rev. Lett. **90**, 151301 (2003) [gr-qc/0110012]
  - [2] C.B. Collins and S.W. Hawking, Astrophys. J. **180**, 317 (1973)
  - [3] J. D. Barrow and M. S. Turner, Nature **292**, 35 (1981)
  - [4] J.D. Barrow, Quart. J. Roy. Astron. Soc. **23**, 344 (1982)
  - [5] R.M. Wald, Phys. Rev. D **28**, 2118 (1983)
  - [6] G. Steigman and M. S. Turner, Phys. Lett. B **128**, 295 (1983).
  - [7] A. A. Starobinsky, JETP Lett. **37**, 66 (1983)
  - [8] M. Demianski, Nature, **307**, 140 (1984).
  - [9] T. Rothman and M. S. Madsen, Phys. Lett. B **159**, 256 (1985).
  - [10] O. Gron, Phys. Rev. D **32**, 1586 (1985) [Erratum-ibid. D **34**, 664 (1986)].
  - [11] M. S. Turner and L. M. Widrow, Phys. Rev. Lett. **57**, 2237 (1986).
  - [12] E. Martinez Gonzalez and B. J. T. Jones, Phys. Lett. B **167**, 37 (1986).
  - [13] L. G. Jensen and J. A. Stein-Schabes, Phys. Rev. D **34**, 931 (1986).
  - [14] T. Rothman and G. F. R. Ellis, Phys. Lett. B **180**, 19 (1986).
  - [15] I. Moss and V. Sahni, Phys. Lett. B **178**, 159 (1986)
  - [16] A. Raychaudhuri and B. Modak, Class. Quant. Grav. **5**, 225 (1988)
  - [17] A.B. Burd and J.D. Barrow, Nuc. Phys. B **308**, 929 (1988)
  - [18] L. H. Ford, Phys. Rev. D **40**, 967 (1989)
  - [19] L. Campanelli, Phys. Rev. D **80**, 063006 (2009) [arXiv:0907.3703 [astro-ph.CO]]
  - [20] R. Maartens, V. Sahni and T. D. Saini, Anisotropy dissipation in brane world inflation, Phys. Rev. D **63**, 063509 (2001) [arXiv:0011105[gr-qc]].
  - [21] J. D. Barrow and S. Hervik, Phys. Rev. D **73**, 023007 (2006) [gr-qc/0511127]
  - [22] C. Pitrou, T. S. Pereira and J. P. Uzan, Predictions from an anisotropic inflationary era, JCAP **0804**, 004 (2008) [arXiv:0801.3596 [astro-ph]].
  - [23] A. E. Gumrukcuoglu, L. Kofman and M. Peloso, Phys. Rev. D **78**, 103525 (2008) [arXiv:0807.1335 [astro-ph]]
  - [24] J. D. Barrow and S. Hervik, Phys. Rev. D **81**, 023513 (2010) [arXiv:0911.3805 [gr-qc]]
  - [25] M. -a. Watanabe, S. Kanno and J. Soda, Phys. Rev. Lett. **102**, 191302 (2009) [arXiv:0902.2833 [hep-th]]
  - [26] A. Ashtekar and P. Singh, Class. Quant. Grav. **28**, 213001 (2011) [arXiv:1108.0893 [gr-qc]].

- [27] A. Ashtekar, T. Pawłowski and P. Singh, Phys. Rev. Lett. **96** 141301 (2006), [arXiv:0602086[gr-qc]].
- [28] A. Ashtekar, T. Pawłowski and P. Singh, Phys. Rev. **D73** 124038 (2006) [arXiv:0604013[gr-qc]].
- [29] A. Ashtekar, T. Pawłowski and P. Singh, Phys. Rev. **D74** 084003 (2006) [arXiv:0607039[gr-qc]].
- [30] A. Ashtekar, T. Pawłowski, P. Singh and K. Vandersloot, Phys. Rev. **D75** 0240035 (2006) [arXiv:0612104[gr-qc]].
- [31] L. Szulc, W. Kaminski and J. Lewandowski, Class. Quant. Grav. **24**, 2621 (2007) [gr-qc/0612101].
- [32] W. Kaminski and J. Lewandowski, Class. Quant. Grav. **25**, 035001 (2008) [arXiv:0709.3120 [gr-qc]]
- [33] A. Ashtekar, A. Corichi, P. Singh, Phys. Rev. D **77**, 024046 (2008) [arXiv:0710.3565 [gr-qc]].
- [34] K. Vandersloot, Phys. Rev. D **75** 023523 (2007) [arXiv:0612070[gr-qc]].
- [35] L. Szulc, Class. Quant. Grav. **24** 6191 (2007)
- [36] E. Bentivegna and T. Pawłowski, [arXiv:0803.4446 [gr-qc]].
- [37] W. Kaminski and T. Pawłowski, Phys. Rev. **D81** 024014 (2010) [arXiv:0912.0162 [gr-qc]].
- [38] T. Pawłowski and A. Ashtekar, Phys. Rev. D **85**, 064001 (2012) [arXiv:1112.0360 [gr-qc]].
- [39] A. Ashtekar and E. Wilson-Ewing, Phys. Rev. **D79** 083535 (2009) [arXiv:0903.3397 [gr-qc]].
- [40] D. W. Chiou, Phys. Rev. D **75**, 024029 (2007) [arXiv:0609029[gr-qc]].
- [41] M. Martin-Benito, G. A. Mena Marugan and T. Pawłowski, Phys. Rev. D **78**, 064008 (2008) [arXiv:0804.3157 [gr-qc]].
- [42] A. Ashtekar and E. Wilson-Ewing, Phys. Rev. D **80**, 123532 (2009) [arXiv:0910.1278 [gr-qc]].
- [43] E. Wilson-Ewing, Phys. Rev. D **82**, 043508 (2010) [arXiv:1005.5565 [gr-qc]].
- [44] A. Ashtekar, T. Pawłowski, P. Singh, Pre-inflationary dynamics in loop quantum cosmology (To appear).
- [45] J. Willis, On the low energy ramifications and a mathematical extension of loop quantum gravity. Ph.D. Dissertation, The Pennsylvania State University (2004).
- [46] V. Taveras, “Corrections to the Friedmann Equations from LQG for a Universe with a Free Scalar Field,” Phys. Rev. D **78**, 064072 (2008) [arXiv:0807.3325 [gr-qc]].
- [47] M. Martin-Benito, G. A. Mena Marugan and T. Pawłowski, Phys. Rev. D **80** 084038 (2009) [arXiv:0906.3751 [gr-qc]].
- [48] L. Szulc, Phys. Rev. D **78**, 064035 (2008)
- [49] P. Singh, Class. Quant. Grav. **29** (2012) 244002 [arXiv:1208.5456[gr-qc]]
- [50] D. Brizuela, D. Cartin and G. Khanna, SIGMA **8**, 001 (2012) [arXiv:1110.0646 [gr-qc]]
- [51] A. Ashtekar and T. A. Schilling, Geometrical formulation of quantum mechanics, gr-qc/9706069.
- [52] A. Corichi and P. Singh, “A Geometric perspective on singularity resolution and uniqueness in loop quantum cosmology,” Phys. Rev. D **80**, 044024 (2009) [arXiv:0905.4949 [gr-qc]].
- [53] B. Gupt and P. Singh, “Contrasting features of anisotropic loop quantum cosmologies: The Role of spatial curvature,” Phys. Rev. D **85**, 044011 (2012) [arXiv:1109.6636 [gr-qc]].
- [54] P. Singh, “Are loop quantum cosmos never singular?,” Class. Quant. Grav. **26**, 125005 (2009) [arXiv:0901.2750 [gr-qc]].
- [55] P. Singh and F. Vidotto, “Exotic singularities and spatially curved Loop Quantum Cosmology,” Phys. Rev. D **83**, 064027 (2011) [arXiv:1012.1307 [gr-qc]].
- [56] P. Singh, “Curvature invariants, geodesics and the strength of singularities in Bianchi-I loop quantum cosmology,” Phys. Rev. D **85**, 104011 (2012) [arXiv:1112.6391 [gr-qc]].
- [57] P. Singh, K. Vandersloot and G. V. Vereshchagin, Phys. Rev. D **74**, 043510 (2006) [arXiv:0606032[gr-qc]].
- [58] X. Zhang and Y. Ling, JCAP **0708**, 012 (2007) [arXiv:0705.2656 [gr-qc]].
- [59] M. Artymowski, Z. Lalak and L. Szulc, JCAP **0901**, 004 (2009)
- [60] A. Ashtekar and D. Sloan, Phys. Lett. B **694**, 108 (2010) [arXiv:0912.4093 [gr-qc]].
- [61] R. Herrera, Phys. Rev. D **81**, 123511 (2010) [arXiv:1006.1299 [astro-ph.CO]].
- [62] A. Corichi and A. Karami, Phys. Rev. D **83**, 104006 (2011) [arXiv:1011.4249 [gr-qc]].
- [63] A. Ashtekar and D. Sloan, Gen. Rel. Grav. **43**, 3619 (2011) [arXiv:1103.2475 [gr-qc]].
- [64] E. Ranken and P. Singh, Phys. Rev. D **85**, 104002 (2012) [arXiv:1203.3449 [gr-qc]].
- [65] E. Komatsu *et al.* [WMAP Collaboration], Astrophys. J. Suppl. **192**, 18 (2011) [arXiv:1001.4538 [astro-ph.CO]].
- [66] C. W. Misner, Phys. Rev. Lett., **19** 533 (1967).
- [67] K. C. Jacobs, Astrophys. J. **153**, 661 (1968).
- [68] B. Gupt and P. Singh, Phys. Rev. D **86**, 024034 (2012) [arXiv:1205.6763 [gr-qc]].

- [69] D. W. Chiou and K. Vandersloot, Phys. Rev. D **76**, 084015 (2007) [arXiv:0707.2548 [gr-qc]].
- [70] T. Cailleteau, P. Singh and K. Vandersloot, Phys. Rev. D **80**, 124013 (2009) [arXiv:0907.5591 [gr-qc]].
- [71] A. Corichi, A. Karami and E. Montoya, Loop Quantum Cosmology: Anisotropy and singularity resolution, arXiv:1210.7248 [gr-qc].
- [72] I. Agullo, A. Ashtekar and W. Nelson, Phys. Rev. Lett. **109**, 251301 (2012) [arXiv:1209.1609 [gr-qc]].
- [73] I. Agullo, A. Ashtekar and W. Nelson, The pre-inflationary dynamics of loop quantum cosmology: Confronting quantum gravity with observations, [arXiv:1302.0254 [gr-qc]].